minerals

MDPI

Article

Sulfide Trace Element Signatures and S- and Pb-Isotope Geochemistry of Porphyry Copper and Epithermal Gold-Base Metal Mineralization in the Elatsite–Chelopech Ore Field (Bulgaria)

Elitsa Stefanova [1,*], Stoyan Georgiev [1], Irena Peytcheva [1], Peter Marchev [1], Albrecht von Quadt [2], Raya Raicheva [1], Ianko Gerdjikov [3], Kalin Kouzmanov [4], Adrian Boyce [5] and Torsten Vennemann [6]

1 Bulgarian Academy of Sciences, Geological Institute "Strashimir Dimitrov", 1113 Sofia, Bulgaria; kantega@abv.bg (S.G.); impeytcheva@gmail.com (I.P.); pmarchev@geology.bas.bg (P.M.); raya@geology.bas.bg (R.R.)
2 Department of Earth Sciences, ETH Zurich, 8092 Zurich, Switzerland; albrecht.vonquadt@erdw.ethz.ch
3 Department of Geology, Paleontology and Fossil Fuels, Sofia University "St. Kliment Ohridski", 1504 Sofia, Bulgaria; ian.gerdjikov@gmail.com
4 Department of Earth Sciences, University of Geneva, CH-1205 Geneva, Switzerland; kalin.kouzmanov@unige.ch
5 Scottish Universities Environmental Research Centre, University of Glasgow, Rankine Avenue, East Kilbride G75 OQF, UK; adrian.boyce@glasgow.ac.uk
6 Institute of Earth Surface Dynamics, University of Lausanne, CH-1015 Lausanne, Switzerland; torsten.vennemann@unil.ch
* Correspondence: elitsa.s@gmail.com

Abstract: The Elatsite–Chelopech ore field in the northern part of the Panagyurishte district in Central Bulgaria comprises numerous spatially associated porphyry copper and epithermal gold deposits and prospects. In addition to the mineralization and alteration features, trace elements, lead and sulfur isotope signatures of sulfide minerals from porphyry copper, base metal and gold-base metal deposits/prospects have been studied. LA-ICP-MS analyses of pyrite, arsenopyrite and sulfosalt minerals validate them as major carriers for Au, Ag, Sb, Se and Co. Pyrite from the three types of mineralization has specific geochemical characteristics. Pyrite from the porphyry copper deposits/prospects has generally lower total trace element content compared to pyrite from the epithermal prospects, except for Se, Co and Ni. Pyrite from the base metal and gold-base metal veins is enriched in As, Au, Ag, Sb and Pb. In pyrite from the base metal deposits, Co and Ni have contents comparable to the pyrite from the porphyry copper deposits, while pyrite from the gold-base metal veins shows lower Co and Ni. Arsenopyrite from these deposits shows similar features. Similarly, sphalerite from the gold-base metal veins also has lower Co content compared to sphalerite from the base metal veins but higher In and Cu contents. In addition to the close spatial relationships between the Elatsite and Gorna Kamenitsa porphyry Cu deposits and Negarstitsa-West and Dolna Kamenitsa base metal prospects, as well as similarities in the mineralization and alteration styles, the lead isotopic ($^{206}Pb/^{204}Pb$ = 18.61–18.68, $^{207}Pb/^{204}Pb$ = 15.64–15.65 for porphyry and $^{206}Pb/^{204}Pb$ = 18.55–18.67, $^{207}Pb/^{204}Pb$ = 15.64–15.68 for base metal) and sulfur isotopic ($\delta^{34}S$ values of −3 to +1‰ for porphyry and $\delta^{34}S$ values of −1.7 to +3.5‰ for base metal) signatures of sulfides support the idea of a genetic link between these two types of deposits. The porphyry and base-metal mineralization result from a common major ore-forming event during the Late Cretaceous, corresponding to deep/higher-temperature and shallower/distal/lower-temperature environments, respectively. In particular, more radiogenic lead ($^{206}Pb/^{204}Pb$ = 18.41–18.47, $^{207}Pb/^{204}Pb$ = 15.67–15.76) and slightly different sulfur isotopic compositions ($\delta^{34}S$ values of +3.5 to +10.6‰) of sulfides from the distal gold-base metal veins of Kordunsko Dere, Svishti Plaz and Shipkite might be a consequence of the interaction of the ore-forming fluids with an external older crustal and isotopically positive S source. Alternatively, a different fluid source/event for the formation of these gold-base metal veins may be suggested.

Citation: Stefanova, E.; Georgiev, S.; Peytcheva, I.; Marchev, P.; von Quadt, A.; Raicheva, R.; Gerdjikov, I.; Kouzmanov, K.; Boyce, A.; Vennemann, T. Sulfide Trace Element Signatures and S- and Pb-Isotope Geochemistry of Porphyry Copper and Epithermal Gold-Base Metal Mineralization in the Elatsite–Chelopech Ore Field (Bulgaria). *Minerals* **2023**, *13*, 630. https://doi.org/10.3390/min13050630

Academic Editors: Guoxue Song, Mingjian Cao, Wenyuan Liu and Chao Zhao

Received: 1 April 2023
Revised: 26 April 2023
Accepted: 27 April 2023
Published: 30 April 2023

Keywords: Elatsite–Chelopech; porphyry copper; polymetallic mineralization; gold-base metal veins; trace elements in sulfide minerals; lead and sulfur isotopes

1. Introduction

Porphyry copper deposits occur within volumes of hydrothermally altered rock in the order of several cubic km that may also contain skarn, carbonate-replacement, sedimentary-hosted and epithermal mineralization. The alteration and economic mineralization in this environment show a general outward and upward zonation from the porphyritic intrusion [1]: porphyry Cu-Mo-Au and/or skarn deposits occur deeper and proximal to causative intrusions, whereas their shallower parts tend to host epithermal mineralization commonly enriched in precious metals, Cu, Pb and Zn. A genetic link between porphyry Cu and adjacent high- or intermediate-sulfidation epithermal mineralization is commonly suggested, based mainly on the geochronology of alteration and mineralization, as well as on fluid inclusion data and isotopic tracing (e.g., [1–6]). In the southern part of the Panagyurishte district, Kouzmanov et al. [2] have demonstrated a genetic link between the Vlaikov Vryh porphyry Cu and the neighboring Elshitsa epithermal Cu-Au deposits, based on the Pb isotopic composition of sulfide minerals and absolute geochronology.

During the last few decades, the development of high-sensitivity and high spatial resolution microanalytical techniques, such as laser ablation inductively coupled mass spectrometry (LA-ICP-MS), has allowed for accurate determination of a large number of trace elements down to the parts-per-billion (ppb) level in many mostly fine-grained hydrothermal minerals (e.g., pyrite, magnetite, chlorite and epidote). Geochemical signatures of these minerals can be successfully used for mineral exploration purposes, owing to certain systematic spatial patterns with respect to fluid source(s) and temperature during alteration (e.g., [7–11]). Pyrite is especially appropriate for such studies because it is commonly the most abundant sulfide mineral in altered rocks from any kind of hydrothermal ore deposit (e.g., [12–14]). Pyrite is also a versatile target mineral because it is a major host of many siderophile and some chalcophile trace elements including many of the pathfinders used in exploration geochemistry: Co, Ni, Cu, As, Sb, Se, Te, Pb, Bi, Mo, Ag, Au and the PGE (e.g., [14–16]) and can be a major and economically important repository of these elements (e.g., [13,17,18]).

The Elatsite–Chelopech ore field, northern Panagyurishte district, Bulgaria, comprises numerous spatially associated porphyry copper and epithermal copper/base metal-gold deposits and occurrences. Most of these are known or inferred to relate to Late Cretaceous calc-alkaline arc magmatism, whereas some prospects are inferred to relate to the extensive Carboniferous magmatism that forms the local basement (e.g., Svishti Plaz; Amov et al. [19]). The occurrences include regular porphyry Cu deposits and base metal-rich and gold-base metal epithermal styles. This diversity of mineralization styles belonging to the greater porphyry Cu environment makes the Elatsite–Chelopech area an excellent place to investigate the possible genetic connections (or lack thereof) between parts of the architecture of the greater porphyry copper to epithermal environment. The correct interpretation of these genetic connections is relevant to the exploration for resources of Cu and byproduct metals. Toward that goal, the aims of our present study are: (1) to document the trace element composition of sulfides in these occurrence types and evaluate their potential utility in exploration, and (2) to use the sulfur and lead isotope signatures of the sulfide minerals as evidence to support or deny the genetic relationship between the occurrences.

2. Geological Setting

The Elatsite–Chelopech ore field is situated in the Panagyurishte District of the Central Srednogorie Zone, Bulgaria. The Srednogorie Zone is part of the Apuseni–Banat–Timok–Srednogorie Arc [20,21] (Figure 1); a belt of mafic to dacitic calc-alkaline magmatism related

to the subduction of Mesozoic oceanic crust under southeastern Europe from the Albian to the Maastrichtian [22]. The Panagyurishte District is a NNW–SSE trending alignment of ore deposits oblique to the general strike of Central Srednogorie Zone. It includes porphyry Cu deposits (Vlaykov Vruh, Tsar Assen, Medet, Assarel, and Elatsite), and high-intermediate sulfidation epithermal deposits (Elshitsa, Radka, Krassen and Chelopech) (Figure 1).

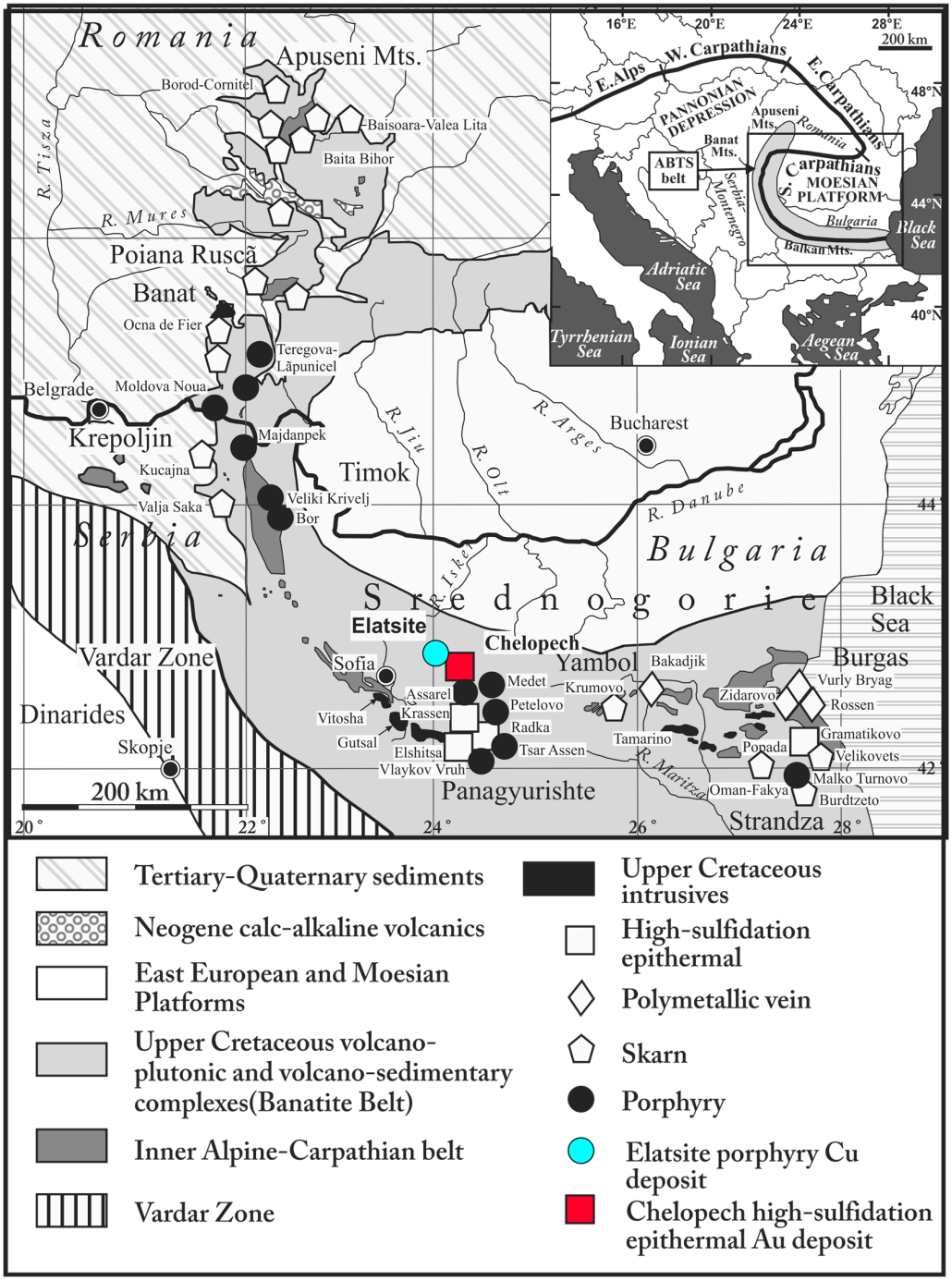

Figure 1. Geological sketch map of part of southeastern Europe showing Late Cretaceous magmatic provinces and the distribution of the main types of ore deposits in the Apuseni–Banat–Timok–Srednogorie (ABTS) belt (modified from Coubanu et al. [20]). Inset: Location of the ABTS belt within the Alpine–Balkan–Carpathian–Dinaride orogenic system (after Heinrich and Neubauer [21]).

The study area is located at the northern end of the Panagyurishte District. The basement consists of pre-Mesozoic metamorphic and igneous rocks, and the post-Srendogorie

cover consists of Quaternary terrestrial sediments (Figure 2). The pre-Mesozoic basement comprises ortho- and para-gneisses and orthoamphibolites of the Paleozoic high-grade Metamorphic Complex [23] and low-grade Ordovician-Silurian meta-sediments of the Phyllite Complex [24]. Numerous post-Variscan granitoids intruded the metamorphic basement and range from gabbrodiorite to granite [23,25–27]. The emplacement of the Carboniferous Vezhen Pluton caused contact metamorphism in the phyllites, forming hornfelsses and mottled schists. Mafic and intermediate dykes and stocks also intruded into the pluton and in the basement during the Carboniferous [24], and mafic enclaves are observed among the granodiorite phases of the pluton. The latter observation has been interpreted as evidence of magma chamber recharge and mingling processes comparable to those invoked as important in porphyry copper genesis (e.g., [1,28]), and it provides some context to the hypothesis that some of the mineralization in the study area may have occurred before the Srednogorie magmatism.

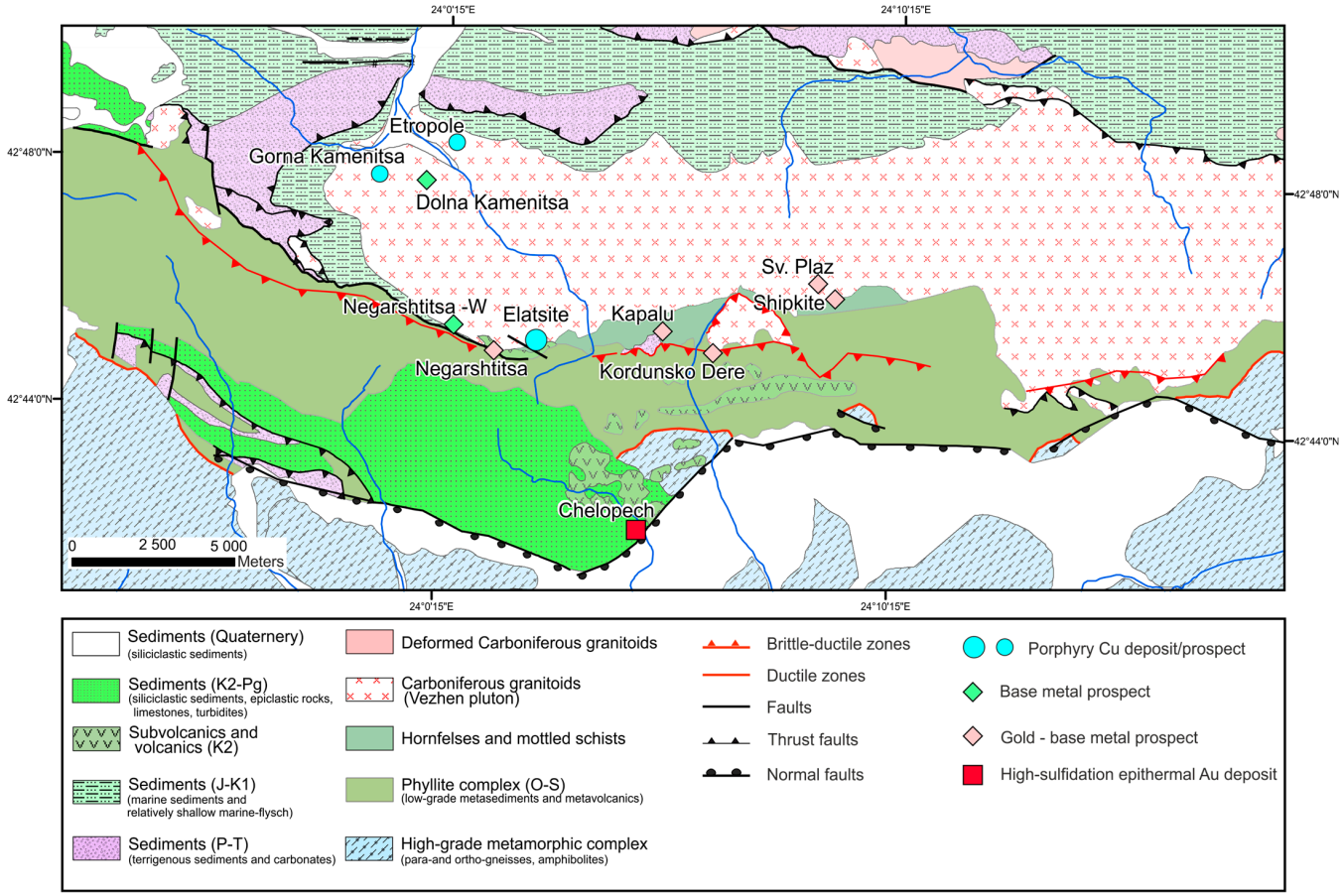

Figure 2. Geological map of the region with the location of the ore deposits and prospects (modified after Antonov et al. [29], Kounov et al. [30] and reference therein).

The Upper Paleozoic–Mesozoic sedimentary sequence consists of Permian to Lower Triassic continental terrigeneous sediments that grade upward into carbonate rocks of the Middle and Upper Triassic ([30] and references therein). Above these, Lower and Middle Jurassic transgressive marine sediments grade upward into a relatively shallow-marine flysch sequence of the Upper Jurassic to Lower Cretaceous.

In the early Cretaceous, brittle–ductile shear zones and thrust faults were formed along the contact between the high-grade Metamorphic Complex and the overlying Mesozoic sediments, as well as in the low-grade metasediments (Figure 2, [31–33]). This event corresponds to the first episode of Alpine compression in the Balkanides [34]. The fault zones and fabrics are overlain by Turonian conglomerates and sandstones, which are the

precursor to the Turonian to Maastrichtian volcano–sedimentary sequence, represented by magmatic rocks and intra-arc sandstones, conglomerates, and subordinate deeper water siliciclastic sediments ([35] and references therein; [36]). The Late Cretaceous magmatic rocks consist of hypabyssal porphyritic intrusions and dykes, which are hosted in the metamorphic basement and the granodiorites of the Vezhen pluton. The Late Cretaceous dykes and subvolcanic bodies are predominantly andesitic, quartz–monzodioritic, granodioritic and dioritic in composition [37–41]. Any original volcanic equivalents have been removed by erosion. A second Alpine compressional event affected the area after the Maastrichtian and caused substantial thrust faulting and folding of the Upper Cretaceous sequences [30,42–44].

The Elatsite–Chelopech ore field covers approximately 150 km^2 and is defined as the group of mineral deposits hosted by the block of pre-Alpine rocks exposed north of the major Chelopech Thrust. The field notably includes the operating mines at the porphyry copper deposit at Elatsite and the high sulfidation epithermal deposit at Chelopech. Other porphyry occurrences occur north of Elatsite, and numerous epithermal base metal and gold prospects, while prospects occur along the range to the east, near the southern margin of the Vezhen Pluton (Figure 2). Crystallization of the causative or bracketing magmatic rocks at Elatsite and Chelopech is constrained by zircon U-Pb geochronology to ~93–91 Ma [37,45]. An altered porphyritic granodiorite dyke at Etropole also crystallized at ~91 Ma (Ireland, T, unpublished zircon U-Pb data). The other occurrences in the district are generally assumed to have also formed around this time, except for the Svishti Plaz and Shipkite prospects at the eastern extreme of the district (Figure 2). These have been considered as possibly linked to the Carboniferous magmatic events [19].

3. Samples and Methods

In this study, we provide results for samples from three porphyry copper deposits: Elatsite, Etropole and Gorna Kamenitsa, two base-metal-rich epithermal prospects: Negarshtita-West and Dolna Kamenitsa, adjacent, respectively, to the Elatsite and Gorna Kamenitsa porphyries, and Au–pyrite–rich epithermal prospects at Kordunsko dere, Svishti Plaz-Central and Shipkite (Table 1, Figure 2). The Chelopech deposit was not included in the present study, as it has been the subject of substantial prior work. Chambefort et al. [45] found that the Elatsite porphyry–Cu and the Chelopech high-sulfidation epithermal deposits are related to two distinct upper crustal magmatic reservoirs and cannot be considered as genetically paired despite their temporal proximity.

Polished thin sections were prepared from 70 altered and mineralized samples with well-developed textural characteristics and clear relative age relations between vein types (Supplementary Table S1). Standard transmitted and reflected light microscopy was combined with scanning electron microscopy-backscattered electron imaging (SEM-BSE) for mineral identification and textural correlation between different generations of quartz, sulfide and alteration minerals. Additionally, SEM-BSE imaging was used to select the areas for further geochemical analyses by in situ techniques (SEM-EDS, LA-ICP-MS and sulfur isotope analyses). The SEM used was a JEOL JSM-6610LV (JEOL Ltd., Tokyo, Japan, equipped with BSE, CL, EDS and WDS detectors) housed at Belgrade University. The standards used were as follows: FeS_2 (Fe-Kα, S-Kα); FeAsS (As-Kα); ZnS (Zn-Kα); PbS (Pb-Lα); $CuFeS_2$ (Cu-Kα); Ag metal (Ag-Lα), Sb metal (Sb-Lα) and Co metal (Co-Kα). Analytical conditions were 20 kV acceleration voltage and 5 nA beam current. The LA-ICP-MS system used at the Geological Institute of the Bulgarian Academy of Sciences consists of a 193 nm ArF excimer laser (ATLEX-SI and ATLEX-LR, Germany), combined with an ELAN DRC-e ICP-MS instrument (Perkin Elmer, ON, Canada). The analyses were performed with 25, 35 or 50 μm beam spots and a repetition rate of 6 Hz. The homogeneous energy density on the sample surface was 5–6 J/cm^2. External standardization on the USGS MASS-1 sulfide standard and the NIST glass SRM-610 allows for linear drift correction of the spectrometer and provides relative element concentrations. These element concentrations were transformed into true values by internal standardization (a known concentration of an element,

determined by SEM in our case), using the Matlab®-based SILLS software Version 1.3.2 for data reduction [46].

Table 1. Deposits and prospects studied from the Elatsite–Chelopech ore field, grouped by their mineralizing style. Minerals that were analyzed for major, minor and trace elements, as well as lead and sulfur isotope analyses from different mineralization stages (bold), are given.

Mineralization Type	Mineralization Stages	Minerals Analyzed by SEM-EDS and LA-ICP-MS Methods	Minerals for Pb Isotopes	Minerals for S Isotopes
Porhyry copper deposits and prospects:				
Elatsite (El)	Qz-Mt → Mt-Bn-Cpy → **Qz-Py-Cpy** → Qz-Moly → **Q-Py** → Qz-Gal-Sph → Qz-Cal-Zeol	Py, Cpy		Py, Cpy
Gorna Kamenitsa (GK)	Q-Cpy±Py → Qz-Moly±Rut → **Qz-Py**	Py, Cpy	Py	Cpy
Etropole (Etr)	Qz-Mt → **Qz-Py-Cpy** → Qz-Moly → **Qz-Py** → Qz-Carb	Py, Cpy	Py	Py
Base metal veins:				
Negarshtitsa-West (NW)	**Qz-Py-Ser** → **Qz-Gal-Sph-Cpy-Fr** → Qz-Carb	Py, Cpy, Sph, Fr	Py, Gal	Py, Cpy, Sph, Gal
Dolna Kamenitsa (DK)	**Qz-Py-Aspy-Ser** → **Qz-Gal-Sph-Cpy-Arg-Fr-Pyrg** → Qz-Carb	Py, Aspy, Cpy, Sph,	Gal	Py, Sph, Gal
Gold-base metal veins:				
Kordunsko Dere (KD)	**Qz-Py** → Qz-Ht → **Qz-Gal-Sph-Cpy** → Qz-Carb	Py, Sph	Py, Gal	Py, Sph, Gal
Svishti Plaz-central part (SvP)	**Qz-Py-Aspy** → **Gal-Sph-Cpy-Tn-Au-Chlt** → Carb	Py, Aspy, Sph, Tn		Sph, Gal
Shipkite (Sh)	**Qz-Py-Aspy** → **Gal-Sph-Cpy-Tn-Au-Chlt** → Carb	Py, Sph	Gal	Py, Gal

Abbreviations: Qz—quartz; Mt—magnetite; Bn—bornite, Cpy—chalcopyrite; Moly—molybdenite; Py—pyrite; Gal—galena; Sph—sphalerite; Cal—calcite; Zeol—zeolite; Rut—rutile; Carb—carbonate; Ser—sericite; Fr—freibergite; Aspy—arsenopyrite; Arg—argentite; Pyrg—pyrargirate; Ht—hematite; Tn—tennantite; Chlt—chlorite.

Lead isotope analyses on pyrite and galena were carried out at the Institute of Geochemistry and Petrology of ETH-Zurich, Switzerland. Samples of 50 mg (pyrite) and 10 µg (galena) were digested in sealed 20 mL Teflon beakers with a mixture of 3 mL 6 M HCl and 1 mL concentrated HNO_3 at 180 °C. After conversion of the samples to bromide form, lead was separated by ion exchange chromatography using 0.5 mL AAT 100–200 mesh resin. Procedural blanks were less than 120 pg Pb. Fractions of the purified lead were loaded on Re-filaments using the silica gel technique, and lead isotope ratios were measured on a Thermo Scientific TritonPlus thermal ionization mass spectrometer in static mode. The analytical errors (2σ) were 0.05% for $^{206}Pb/^{204}Pb$, 0.07% for the $^{207}Pb/^{204}Pb$, and 0.1% for the $^{208}Pb/^{204}Pb$.

The sulfide samples for sulfur isotope microanalyses were prepared by crushing and handpicking grains under a binocular microscope. The sulfur isotope compositions were measured at the University of Lausanne, Switzerland on a Nier-type mass spectrometer MS 4/7 with a double collector system, with compensation for the contribution of oxygen isotope variability of the SO_2. Each sample was measured three times, reaching a precision of ±0.2 per mil with respect to the Canyon Diablo meteorite standard (CDT). Additionally, in situ S isotope analyses were performed on pyrite, chalcopyrite, galena and sphalerite using the Nd-YAG laser system at the Scottish Universities Environmental Research Centre (SUERC). The system consists of SPECTRON LASERS 902Q CW Nd-YAG (1-W power), operating in TEM_{00} mode and VG SIRA II gas mass spectrometer. Raw machine data were converted to $\delta^{34}S$ values by calibration with international standards NBS-123 (17.1‰) and IAEA-S-3 (31‰), as well as SUERC's internal lab standard CP-1 (4.6‰). All sulfur isotope compositions were calculated relative to Canon Diablo Troilite (CDT) and are reported in standard notation. Details of the laser characteristics, experimental conditions and methodology are given in Fallick et al. [47].

A combination of atomic absorption analysis (AAA) and inductively coupled atomic emission spectroscopy (ICP-AES) was used to analyze the bulk rock samples. In addition, fused pellets with lithium tetraborate were prepared from hydrothermally altered but less mineralized samples and subsequently measured by LA-ICP-MS to determine the trace element content of the samples. The AAA were performed at the SGA Chelopech laboratory. The ICP-AES measurements were performed at the certified laboratory "Aquateratest" Sofia.

4. Results

4.1. Mineralization and Alteration Styles

4.1.1. Porphyry Cu Deposits/Prospects

At Elatsite, the porphyry hydrothermal paragenesis consists of: early magnetite–quartz; magnetite–bornite–chalcopyrite; pyrite–chalcopyrite; quartz–molybdenite; and late quartz–pyrite, quartz–galena–sphalerite, and quartz–carbonate–zeolite veins [48–52]. Potassic alteration is spatially associated with the mineralization of the quartz–magnetite and magnetite–bornite–chalcopyrite stages, which host the majority of the Pd and Pt in the deposit [48,49,53–55]. The bulk of the Cu inventory corresponds to the pyrite–chalcopyrite stage, and this is associated with both potassic and propylitic alteration assemblages [52]. The quartz–pyrite assemblage is observed mostly as veins with well-defined sericitic alteration halos. Additionally, very late intermediate-sulfidation epithermal veins with sericitic alteration are described in the upper part of the deposit [52,56]. These late veins span the range of mineralogy observed among all the other prospects of the district, and locally include tetrahedrite–freibergite, pyrargyrite, and/or unidentified Bi-Te and Ag-Te minerals in addition to common sulfides [56]. Of these, our Elatsite samples correspond to the pyrite–chalcopyrite stage and quartz–pyrite–(sericite) stage veins.

Mineralization stages in the other two porphyry Cu prospects (Etropole and Gorna Kamenitsa) show some of the features similar to the Elatsite deposit (summarized in Table 1). It is unclear if the simpler apparent paragenesis at these prospects is a real feature or a function of the poorer exposure and availability of materials. The samples analyzed from these locations also correspond to the pyrite–chalcopyrite stage and quartz–pyrite–(sericite) stage veins. In our samples from all three porphyry localities, the pyrite–chalcopyrite stage veins consist mostly of chalcopyrite and pyrite (Figure 3A), with inclusions of tetrahedrite in chalcopyrite. Pyrite and chalcopyrite are also disseminated in the host rocks (Figure 3B). The quartz–pyrite–(sericite) veins consist mostly of quartz and pyrite (Figure 3C) in association with sericite wallrock alteration. Exceptions to this are the sample El1360W from the western margin of the Elatsite deposit, which includes both chalcopyrite and sphalerite, as well as unidentified Pb-Ag-Bi-bearing inclusions in pyrite that were detected by SEM (Figure 3D).

Samples that were collected from between Gorna Kamenitsa porphyry and Dolna Kamenitsa base metal prospects were also studied, as this appears macroscopically as a zone of transition between these two distinct occurrence styles (GDK samples). These samples are from drillhole C26 and from surface outcrops. Some of the drill core samples show a hydrothermal alteration paragenesis typical of porphyry Cu deposits: hydrothermal K-feldspar and biotite with magnetite, propylitic alteration (predominantly epidote and chlorite) and sericitic alteration. The main sulfide minerals are pyrite and chalcopyrite as disseminations or in thin veinlets. However, in some samples, adularia occurs in the quartz–pyrite veins, and small inclusions of chalcopyrite, sphalerite, galena, and Bi-bearing phases accompany the pyrite, suggesting an intermediate or low sulfidation epithermal overprint in these samples. We have analyzed samples from both types of mineralizations.

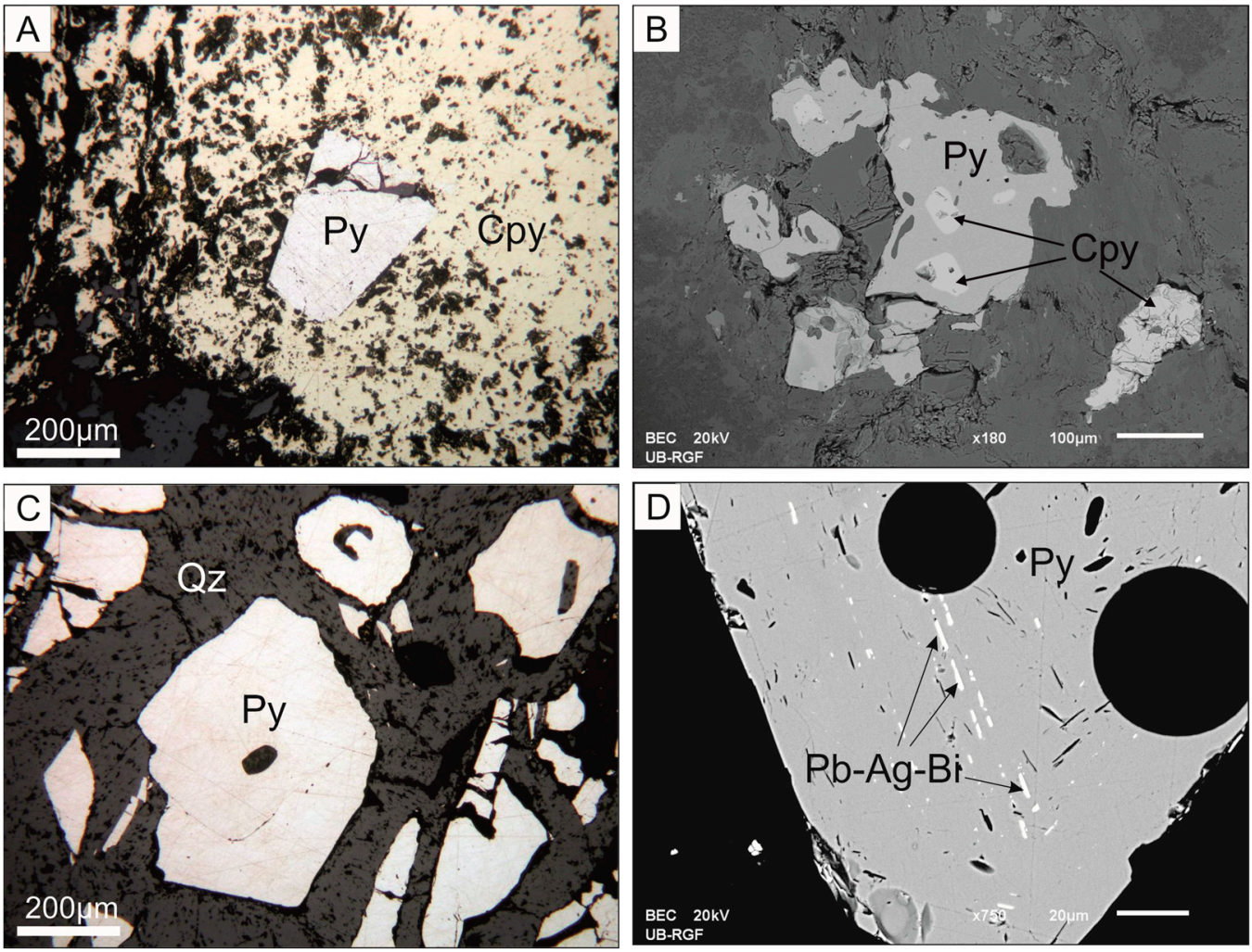

Figure 3. Photomicrographs of samples from porphyry Cu deposit/prospects, showing relationships between observed minerals: (**A**) Chalcopyrite–pyrite vein contains predominantly chalcopyrite and rare pyrite crystals (sample El1060S7). (**B**) Disseminated chalcopyrite and pyrite (GK13-2b). (**C**) Quartz–pyrite vein with subhedral pyrite crystals (El1300E35). (**D**) Unidentified Pb-Ag-Bi inclusions in pyrite from quartz–pyrite–sericite stage (El1360W-2). The holes are laser craters. Abbreviations: Py—pyrite; Cpy—chalcopyrite; Qz—quartz.

4.1.2. Base Metal Veins

In the two base metal prospects studied, sericitic alteration overprints propylitic alteration. There is a simple sulfide paragenesis of Fe-(As) sulfides, followed by base metal sulfides and sulfosalts. In the early stage, subhedral to euhedral pyrite (Figure 4A) occurs in association with quartz and sericite. Notable variations on this include pyrite crystals with euhedral cores and sieve-like rims at Negarshtitsa-West (Figure 4B) and pyrite associated with marcasite or arsenopyrite at Dolna Kamenitsa. SEM-BSE imagery reveals that pyrite has patchy zoning (Figure 4C). Sulfides of the early stage were fractured and infilled by the later base metal stage, which includes a diverse assemblage of sphalerite, chalcopyrite, galena, freibergite, tennantite, argentite, pyrargyrite, and rarely native Ag (Figure 4D,E). On the SEM-BSE images, freibergite shows zonal textures (Figure 4F). No gold was observed microscopically. Quartz–carbonate ± chlorite veins are later and cut earlier formed quartz-sulfide veins. Our samples from these veins represent the quartz–pyrite ± arsenopyrite and base metal stages.

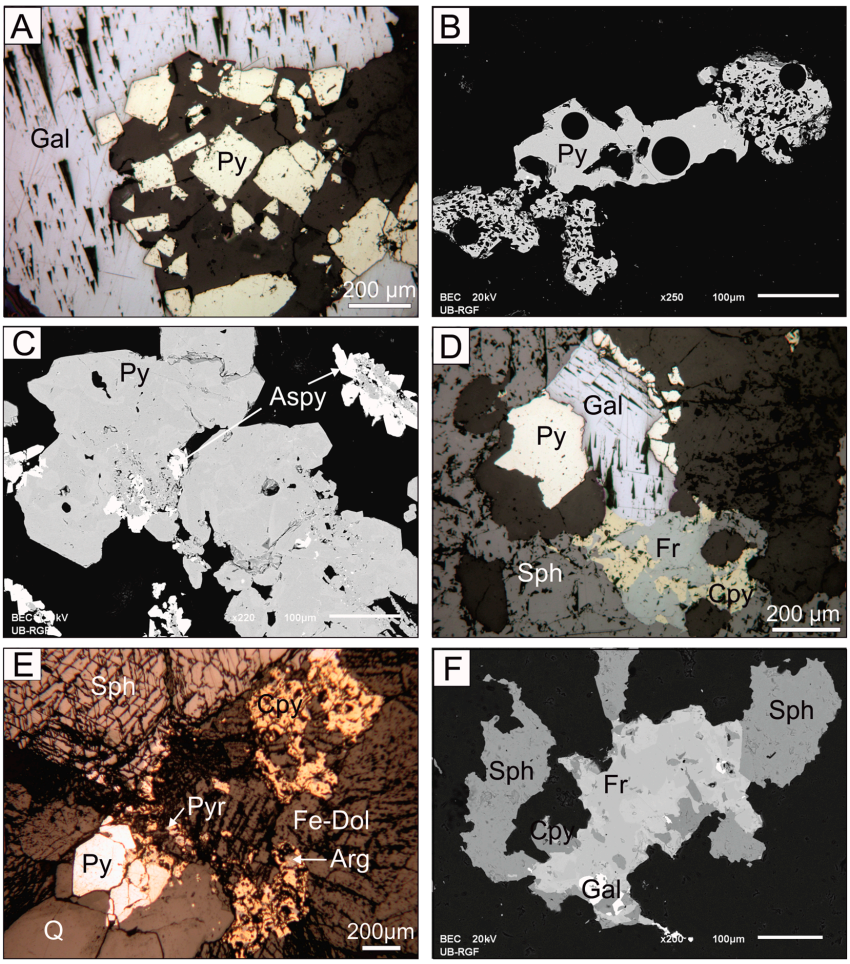

Figure 4. Photomicrographs of samples from base metal prospects, showing relationships between observed minerals: (**A**) Subhedral to euhedral pyrite crystals and later galena (H-C1_183.9). (**B**) Pyrite with massive core and sieve-textured rims (H-C 1_21). (**C**) Pyrite with irregular zoning in association with arsenopyrite (DK12-1). (**D**) Sphalerite, galena, chalcopyrite and freibergite from the base metal stage around earlier-formed pyrite grain (H-C 1_183.9). (**E**) Pyrite grains are cracked. Chalcopyrite, sphalerite, galena, pyrargyrite and argentite in the cracks. Later carbonates (DK12-1). (**F**) Irregular zoning of freibergite (H-C 1_177.8). Abbreviations: Py—pyrite; Aspy—arsenopyrite; Cpy—chalcopyrite; Gal—galena; Sph—sphalerite; Fr—freibergite; Pyr—pyrargyrite; Arg—argentite; Qz—quartz.

4.1.3. Gold-Base Metal Veins

Similarly to the base metal prospects here, the most intense alteration type is sericitization. In the area of Kordunsko Dere where metabasites are present, a propylitic alteration is also observed. The earliest-formed sulfide is pyrite, with subhedral to euhedral morphology, reaching up to 500 µm in size. Often, it precipitates together with arsenopyrite. Thin quartz–hematite veinlets cut earlier pyrite crystals. Pyrite and arsenopyrite crystals were subsequently brecciated during the later gold-base metal stage (Figure 5A,B). Gold-base metal veins consist mostly of galena, sphalerite, chalcopyrite, tennantite and gold often have alteration salvages of chlorite. Small pyrite grains are also typical for these veins. Petrographic observations show that these small pyrite grains are formed by the fragmentation of the earlier-formed large pyrite crystals. The gold is found as rounded inclusions up to 30 µm in galena, sphalerite, pyrite and chalcopyrite (Figure 5C), filling cracks in pyrite and arsenopyrite together with the other sulfide minerals (Figure 5A,B) or in quartz around pyrite and arsenopyrite crystals (Figure 5D,F). In the latter, gold forms irregular elongated

grains up to 150 µm in size. An unidentified Au-Ag-S phase associated with gold grains is also observed on the SEM-BSE images.

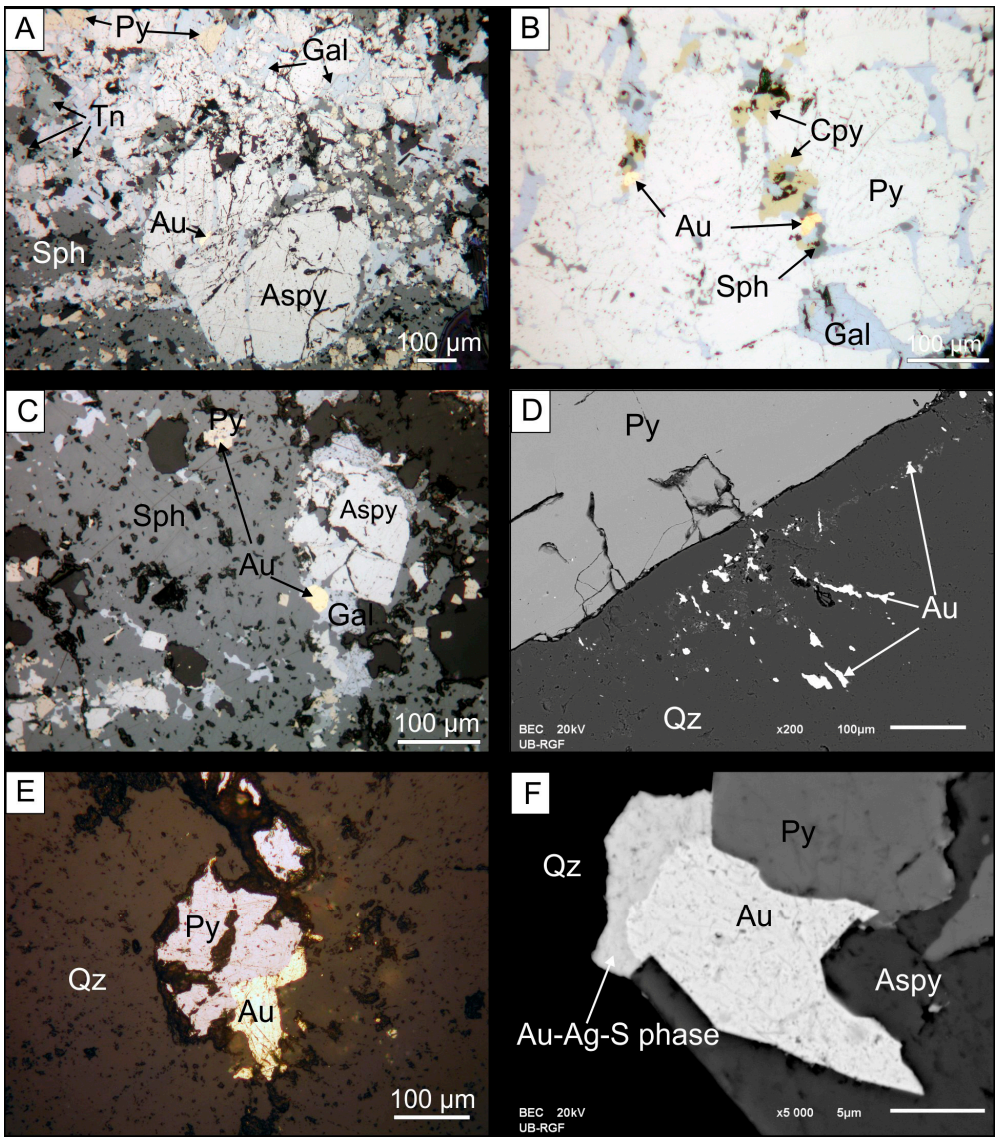

Figure 5. Photomicrographs of samples from gold-base metal prospects, showing relationships between observed minerals: (**A**) Early pyrite and arsenopyrite cracked and brecciated by later sphalerite, galena, chalcopyrite, tennantite and gold (Sh13-8c). (**B**) Galena, sphalerite, chalcopyrite and gold filling fractures in pyrite (Sh1a_127.2). (**C**) Rounded inclusions of gold in galena and pyrite (Sh13-8c). (**D**,**E**) Irregular elongated gold grains in quartz around pyrite crystals (Sh13-6). (**F**) Unidentified Au-Ag-S phase around gold grain (Sh13-8a). Abbreviations: Py—pyrite; Aspy—arsenopyrite; Cpy—chalcopyrite; Gal—galena; Sph—sphalerite; Tn—tennantite; Au—gold; Qz—quartz.

Quartz–carbonate, rutile ± chlorite assemblage was later, and it is found as thin veinlets as well as in voids of early veins. The samples analyzed from these locations correspond to the early pyrite–arsenopyrite stage and the later gold-base metal stage.

4.2. Whole-Rock and Mineral Chemistry

The results from atomic absorption analysis are reported in Supplementary Table S2, and those from ICP-AES and LA-ICP-MS analyses are combined in Supplementary Table S3. From the Elatsite porphyry Cu deposit, only samples from the quartz–pyrite stage with

sericitic alteration from the upper marginal parts of the open pit were analyzed. All studied samples from the three porphyry Cu deposit/prospects have relatively low Cu content (max. 1650 ppm), and low As (up to 48 ppm), Pb (below 120 ppm) and Zn (below 225 ppm). The highest Mo content of 190 ppm was measured in a sample from Gorna Kamenitsa. The Au content in the samples from the Elatsite deposit is up to 0.59 ppm.

Five samples from base metal prospects were analyzed for whole rock geochemistry. Only two of them show high contents of Zn (up to 18.05%) and Pb (up to 1.3%). Gold is also detected (up to 2.44 ppm in a sample from Dolna Kamenitsa), and Ag is up to 33 ppm and Cu is below 442 ppm.

The samples between Gorna Kamenitsa porphyry Cu and Dolna Kamenitsa base metal prospects have variable metal contents: Cu (30–321 ppm); Zn (11–311 ppm); Pb (6.55–990 ppm); Ag (0.67–6.52 ppm) and Au (<0.01–4.99 ppm).

Most of the analyzed samples from the gold-base metal prospects consist of massive ore, and they show very high metal and semi-metal contents: Cu (up to 7633 ppm); Zn (up to 16.3%), Pb (up to 16.2%), As (up to 2.76%), Ag (up to 230 ppm) and Au (up to 214.6 ppm). The samples with high Zn content also show elevated Cd values.

Pyrite from all deposit/prospects was analyzed systematically by SEM-EDS and LA-ICP-MS, while all the other sulfide and sulfosalt minerals were measured sporadically, and there are only a limited number of analyses available. Analyses for all measured minerals are reported in Supplementary Tables S4 and S5, as well as in Figures 6 and 7A,B for pyrite + arsenopyrite and sphalerite, respectively.

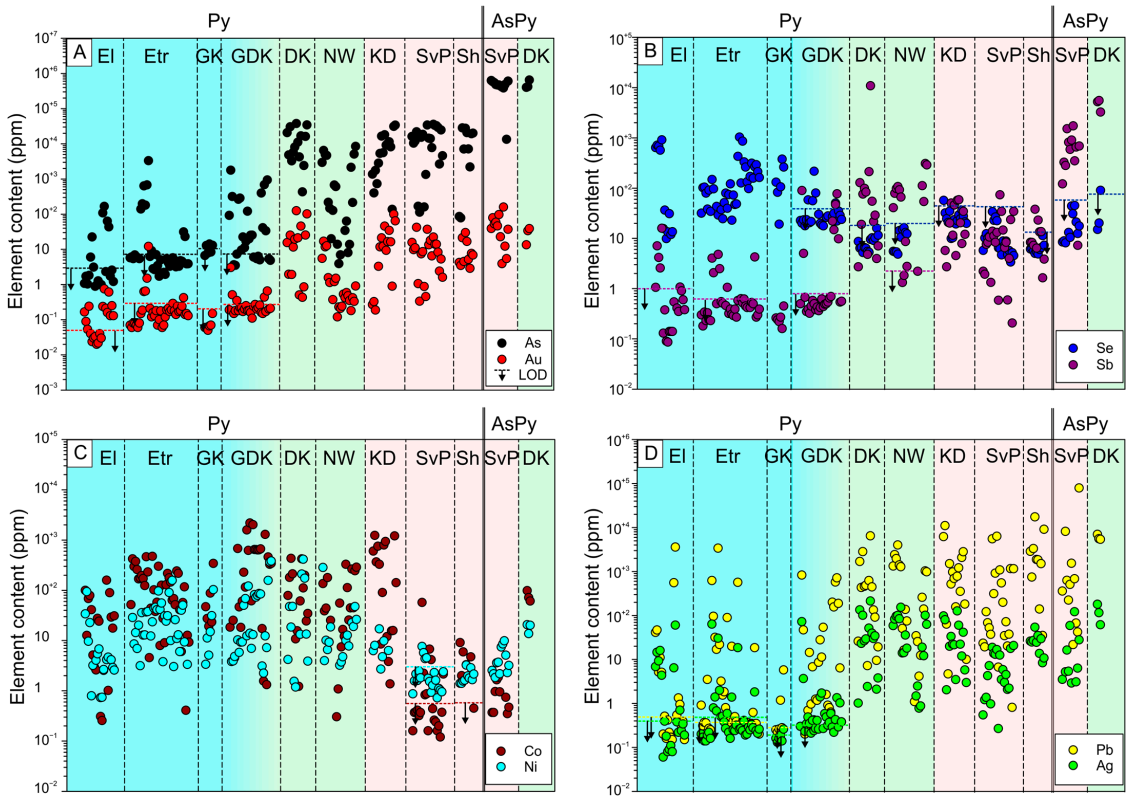

Figure 6. Element content in pyrite from all studied deposit/prospects and arsenopyrite where present obtained by LA-ICP-MS analyses. Deposit/prospects are sorted according to their mineralization type—cyan color for porphyry copper; green for base metal; pinkish for gold-base metal. Abbreviations: El—Elatsite; Etr—Etropole; GK—Gorna Kamenitsa; GDK—Gorna-Dolna Kamenitsa; DK—Dolna Kamenitsa; NW—Negarshtitsa-West; KD—Kordunsko Dere; SvP—Svishti Plaz; Sh—Shipkite.

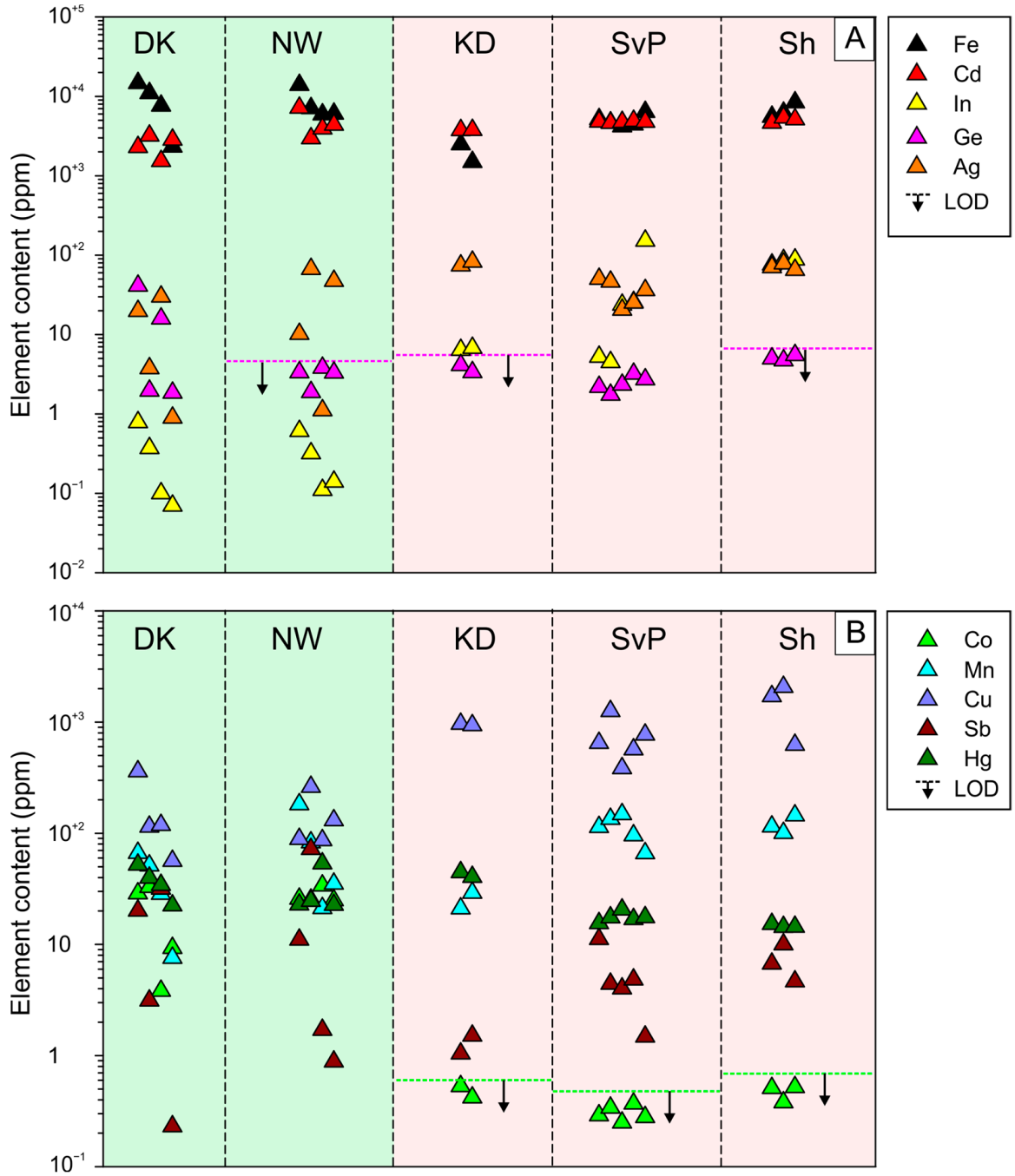

Figure 7. Element content in sphalerite from base metal and gold-base metal prospects obtained by LA-ICP-MS analyses. Prospects are sorted according to their mineralization type. Abbreviations: DK—Dolna Kamenitsa; NW—Negarshtitsa-West; KD—Kordunsko Dere; SvP—Svishti Plaz; Sh—Shipkite.

The composition of pyrite from the three porphyry Cu deposits/prospects is similar. Pyrite is poor in As and Au (often below limit of detection, Figure 6A) and has low Pb, Ag and Sb (Figure 6B,C). In contrast, it is rich in Se (up to 1036 ppm), Co (up to 376 ppm) and Ni (up to 157 ppm) (Figure 6C,D). Like pyrite, measured chalcopyrite from the porphyry Cu type mineralization also has high Se content (up to 412 ppm). The sulfosalt inclusions in chalcopyrite were defined as zincian tetrahedrite. Pyrite from the GDK samples shows strong variations in its trace element content (Figure 6).

Arsenopyrite, chalcopyrite, sphalerite and sulfosalts from the base metal veins were analyzed in addition to pyrite. All pyrite samples from Dolna Kamenitsa correspond to arsenian pyrite (As content up to 3.4 wt%), enriched in Au (up to 125 ppm) (Figure 6A). Irregular zones in pyrite crystals that were observed on the BSE images show variable As content. The zones with higher As content also have higher Au values. Most of the pyrite samples from the Negarshtitsa-West prospect are also As- and Au-bearing. An exception is the pyrite from a sample with intense sericitic alteration where pyrite has massive inner and sieve-textured outer parts. This pyrite has low As content, and Au is below LOD (<0.16 ppm). The sieve-textured zones of the pyrite have higher Bi, Pb, Ag and Cu contents, compared to the massive inner parts. Small chalcopyrite inclusions are also observed within the porous zones. Pyrite from both base metal prospects is also rich in Co, Ni, Sb, Pb and Ag and has low Se content (Figure 6). Chalcopyrite is also poor in Se and has elevated contents of Pb, Sb and Ag. Arsenopyrite from the Dolna Kamenitsa prospect is Au-rich (up to 39 ppm Au) with high Co, Ni, Cu, Sb, Ag and Pb (Figure 6 A–D).

Most of the analyzed sulfosalts from both prospects are defined as members of the tetrahedrite group with Ag content between 2.56 and 6.10 apfu. These from Negarshtita-West prospect showed zoning on the BSE images due to the variable Cu and Ag contents. As a whole, freibergite is Au-rich, and the zones with higher Ag and lower Cu contents have higher Au. The highest measured Au value is 144 ppm.

The maximum measured FeS content in sphalerite from both prospects is 3.48 mol%. Cadmium content reaches up to 7500 ppm, Cu—up to 360 ppm, Ag—up to 67 ppm, Mn—up to 182 ppm, Co—up to 34 ppm and Hg—up to 53.5 ppm. Germanium and In contents are relatively low (Figure 7).

Pyrite and sphalerite from gold-base metal prospects and the Svishti Plaz-Central part were analyzed; additionally, trace elements in arsenopyrite and sulfosalts were measured. Like the pyrite from the base metal prospect, the pyrite from the three gold-base metal prospects is As- and Au-bearing (Figure 6). It has high Cu, Sb, Pb and Ag and low Se and Ni contents. Cobalt content in the pyrite from Svishti Plaz-Central and Shipkite is very low, while in the pyrite from Kordunsko Dere, it is slightly higher (Figure 6C). Arsenopyrite from the Svishti Plaz-Central part is also Au-rich, has high Cu, Sb, Pb and Ag content and low Co and Ni (Figure 6). The Cu-sulfosalt in this sample was determined as tennantite. We performed only two LA-ICP-MS analyses, and in one of them, gold was detected (5.6 ppm). Cobalt content is very low.

All analyzed sphalerite samples from the three gold-base metal prospects are Fe poor (with FeS content up to 3.11 mol%). The Cd content reaches 5000 ppm, Cu—up to 2000 ppm, Ag—up to 83 ppm, Mn—up to 149 ppm and Hg—up to 44.7 ppm. Germanium is relatively low, while In content varies from 4.5 to 152 ppm (Figure 7).

4.3. Pb Isotopes

The Pb isotope data obtained for the studied sulfides from the Elatsite–Chelopech ore field are listed in Table 2 and plotted in Figure 8.

Table 2. Lead isotope data for sulfides from deposits and prospects of the Elatsite–Chelopech ore field.

№	Sample №	Deposit/Prospect	$^{206}Pb/^{204}Pb$	2σ Error	$^{207}Pb/^{204}Pb$	2σ Error	$^{208}Pb/^{204}Pb$	2σ Error
Porhyry copper deposits and prospects:								
1	KS 13-1 Py	Etropole	18.6150	0.0005	15.6390	0.0004	38.6480	0.0010
2	GK13-2B-Py	Gorna Kamenitsa	18.6856	0.0100	15.6518	0.0084	38.8025	0.0209
Base metal veins:								
3	DK12-1-Gal	Dolna Kamenitsa	18.5514	0.0006	15.6558	0.0007	38.6820	0.0024
4	H-C1-Gal	Negarshtitsa-West	18.5923	0.0009	15.6773	0.0011	38.7235	0.0037
5	H-C1 Py	Negarshtitsa-West	18.6678	0.0095	15.6829	0.0084	38.6678	0.0095
6	Neg 15-1	Negarshtitsa-West	18.5946	0.0041	15.6452	0.0034	38.6393	0.0085
Gold-base metal veins:								
7	KD13-3 Py	Kordunsko Dere	18.4681	0.0009	15.7615	0.0009	38.7561	0.0030
8	KD13-3 Gal	Kordunsko Dere	18.4584	0.0006	15.7512	0.0042	38.7226	0.0050
9	Sh1a-2c-Gal	Shipkite	18.4161	0.0002	15.6832	0.0003	38.5049	0.0009

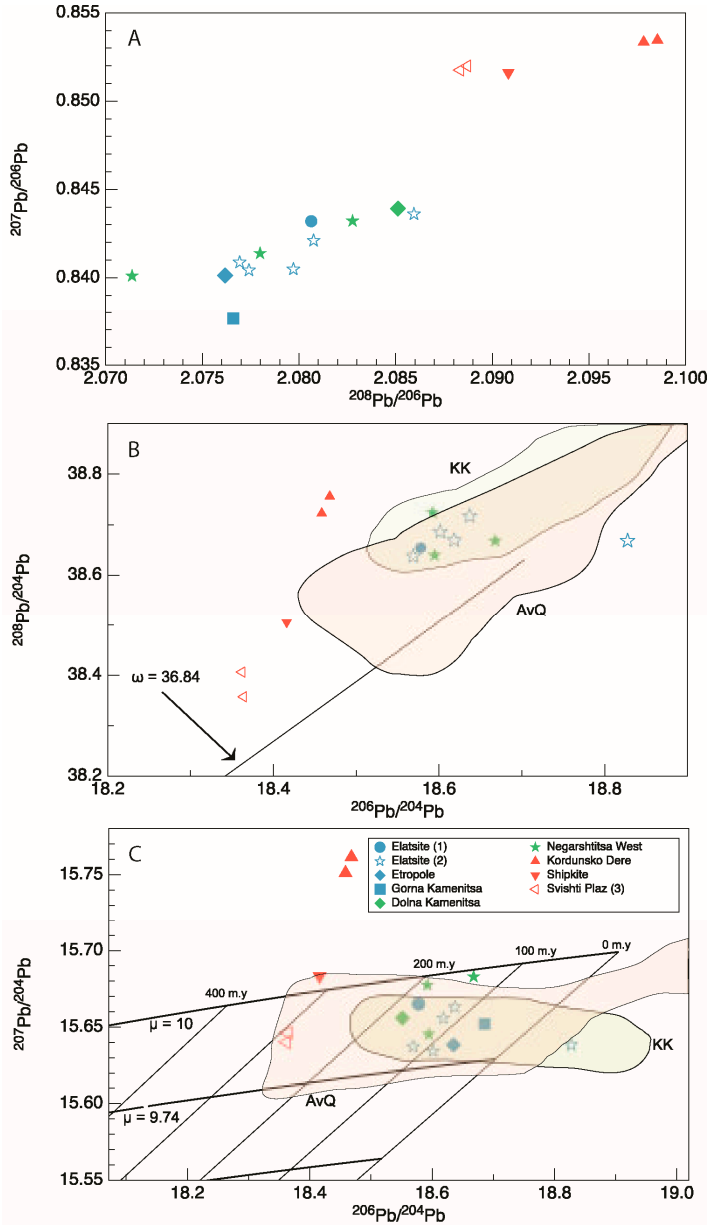

Figure 8. Lead isotope data of sulfides from the Elatsite–Chelopech ore-field (**A**–**C**) compared with published lead isotope whole-rock data for Central Srednogorie/Panagyurishte district (**B**,**C**). (**A**) $^{208}Pb/^{206}Pb$ vs.$^{207}Pb/^{206}Pb$ plot, (**B**) $^{208}Pb/^{204}Pb$ vs. $^{206}Pb/^{204}Pb$ plot and (**C**) $^{207}Pb/^{204}Pb$ vs. $^{206}Pb/^{204}Pb$ plot. The evolutionary Pb-Pb curves for the different μ and ω values are calculated after Stacey and Kramers [57]. The "KK" and "AvQ" fields consist of whole-rock Pb-isotope for Late Cretaceous and Variscan magmatic rocks of the Panaguyrishte district after Kouzmanov et al. [2], and von Quadt et al. [37,38], respectively. All whole-rock samples are not age-corrected. Sulfide lead isotope data from Elatsite (1) are after Amov et al. [19], Elatsite (2) after von Quadt et al. [37], and Svishti Plaz (3) after Amov [58].

On the plots, the Pb isotope data are shown together with published data for sulfides [19,37,58] and of Late Cretaceous and Variscan magmatic rocks from the Central Srednogorie/Panagyurishte district [2,37,38]. The variations in the isotopic compositions of lead clearly separate two groups of deposits. The first group (1) of the porphyry-copper deposit/prospects of Elatsite, Etropole and Gorna Kamenitsa and the base metal veins of Dolna Kamenitsa and Negarshtitsa-West is characterized by more evolved $^{206}Pb/^{204}Pb$ and $^{208}Pb/^{204}Pb$ ratios, but with lower ratios $^{207}Pb/^{204}Pb$. In Figure 8, the corresponding

points are grouped in a small field with a narrow variation of the lead isotope ratios that overlap with the field of the Late Cretaceous magmatic rocks. According to Stacey and Kramers [57], these data infer possible Late Cretaceous model age. The μ ($^{238}U/^{204}Pb$) values between 9.75 and 10.0 suggest an input of Pb from the continental crust. The second group of deposits (2) is represented by the gold-base metal veins of Kordunsko Dere and Shipkite. They reveal lower $^{206}Pb/^{204}Pb$ but higher $^{207}Pb/^{204}Pb$ (15.67–15.76) and suggest a lead contribution from old continental crust. The two groups are also well distinguished in the $^{207}Pb/^{206}Pb$ vs. $^{208}Pb/^{206}Pb$ diagram (Figure 8A).

4.4. S Isotopes

The sulfur isotope composition of pyrite and chalcopyrite from the porphyry copper deposits and occurrences is characterized by $\delta^{34}S$ between −2.5 and +1‰ (Table 3, Figure 9). In sulfides (pyrite, chalcopyrite, sphalerite and galena) from the base metal veins, $\delta^{34}S$ varies in the same range; only the Negarshtitsa West pyrite samples and a chalcopyrite reveal more positive values $\delta^{34}S$ of +2.5 to +2.8, and +3.5‰, respectively. A trend of increasing $\delta^{34}S$ is observed in the sulfide samples from the distal gold-base metal veins that are characterized by $\delta^{34}S$ values of +3.5 to +10.6‰.

Table 3. Whole-mineral (normal font) and in situ (italic) sulfur isotope data of sulfides from deposits and prospects of the Elatsite–Chelopech ore field.

№	Sample	Deposit/Prospect	Mineral	Mean $\delta^{34}S$ (‰)
Porhyry copper deposits and prospects:				
1	*1090 E03*	*Elatsite*	*chalcopyrite*	*−3.0*
2	*1330 EO1*	*Elatsite*	*pyrite*	*1.0*
3	*1330 EO1*	*Elatsite*	*chalcopyrite*	*−1.5*
4	EL12-1	Etropole	pyrite	−2.5
5	*C26-3*	*Gorna Kamenitsa*	*chalcopyrite*	*−1.5*
Base metal veins:				
6	*NEG15-1*	*Negarshtitsa West*	*pyrite*	*2.5*
7	*NEG15-1*	*Negarshtitsa West*	*sphalerite*	*1.0*
8	*NEG15-1*	*Negarshtitsa West*	*galena*	*−1.7*
9	H-C1 (177.8)	Negarshtitsa West	pyrite	2.8
10	*H-C1 (177.8)*	*Negarshtitsa West*	*pyrite*	*2.6*
11	*H-C1 (177.8)*	*Negarshtitsa West*	*chalcopyrite*	*3.4*
12	*H-C1 (177.8)*	*Negarshtitsa West*	*galena*	*0.8*
13	H-C1 (183.8)	Negarshtitsa West	galena	2.8
14	DK12-1	Dolna Kamenitsa	pyrite	0.1
15	*DK12-1*	*Dolna Kamenitsa*	*sphalerite*	*0.5*
16	*DK12-1*	*Dolna Kamenitsa*	*galena*	*6.1*
17	*DK15-1A*	*Dolna Kamenitsa*	*pyrite*	*0.2*
18	*DK15-1A*	*Dolna Kamenitsa*	*sphalerite*	*−0.8*
19	*DK15-1A*	*Dolna Kamenitsa*	*galena*	*0.4*
Gold-base metal veins:				
20	*KD13-3*	*Kordunsko Dere*	*pyrite*	*10.6*
21	KD13-3	Kordunsko Dere	pyrite	6.2
22	*KD13-3*	*Kordunsko Dere*	*sphalerite*	*6.2*
23	KD13-3	Kordunsko Dere	*galena*	4.0
24	*KD13-3*	*Kordunsko Dere*	*galena*	*3.5*
25	*SH13-8A*	*Sv. Plaz-Central part*	*galena*	*6.2*
26	*SH13-8A*	*Sv. Plaz-Central part*	*sphalerite*	*5.2*
27	Sh1a	Shipkite	pyrite	4.5
28	Sh1a	Shipkite	*galena*	3.3

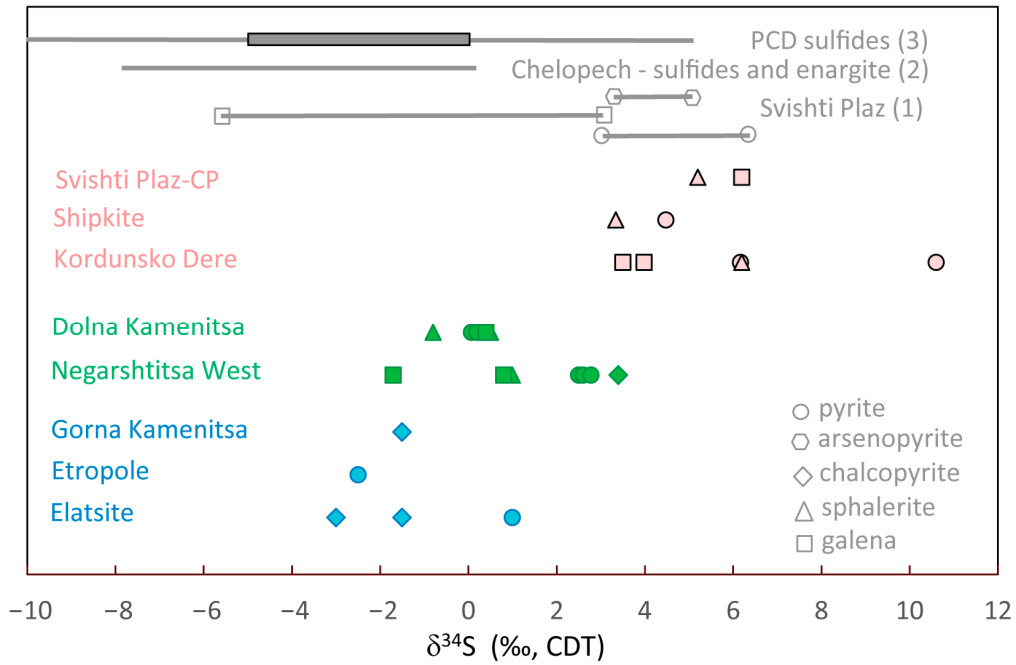

Figure 9. Variations of $\delta^{34}S$ (‰) vs. CDT (Canyon Diablo Troilite) in sulfides from deposits and prospects in the northern part of Elatsite–Chelopech ore field, Bulgaria. For comparison, published sulfur isotope data for the same region of study are shown: (1) Bogdanov and Zairi [59]; (2) Moritz et al. [60]; and the main field of porphyry copper deposits (PCD; black line with the dark grey rectangle of most common variations from 0 to −5 $\delta^{34}S$‰; (3) Hofstra and Cline ([17] and references therein).

5. Discussion

5.1. Porphyry Copper and Proximal Base Metal Deposits/Prospects

Our petrographic observations show that the studied porphyry Cu deposit/prospects share similar alteration and mineralization styles. Special attention was paid to quartz–pyrite–sericite vein samples from the marginal upper west part of Elatsite that have distal position to the copper mineralization but could mark the transition to the closely spatially associated Negarshtitsa-West base metal veins. Texturally and mineralogically, these veins are similar to the pyrite veins from the upper levels of the deposit, described by Mladenova et al. [56]. The authors interpret these veins as intermediate-sulfidation epithermal mineralization. At Negarshtita-West, the samples with intense sericitic alteration consist mainly of pyrite and lesser amounts of chalcopyrite, galena and sphalerite. Pyrite has massive inner and sieve-textured outer parts with chalcopyrite inclusions. Our LA-ICP-MS data show higher Bi, Pb, Cu and Ag content in the porous pyrite. These veins could be analogous to the quartz–pyrite–sericite veins that were studied from the upper western part of the Elatsite deposit. Base metal veins from the Negarshtitsa-West and Dolna Kamenitsa prospects that consist of sphalerite, galena, freibergite, marcasite, and native Ag could be analogous to the base metal veins from the Elatsite deposit, described by Mladenova et al. [56] and Gonzalez-Gimenez et al. [55].

Although the whole-rock geochemistry shows that these samples from the base metal veins contain up to 3.72 ppm Au, microscopically native gold was not observed. LA-ICP-MS analyses reveal that As-bearing pyrite, as well as arsenopyrite and sulfosalts, contain gold. Growth zoning of the pyrite observed on the BSE images is controlled by the variable arsenic content. A positive correlation between the As and Au content in pyrite exists. Similarly, there is a positive correlation between Ag and Au in zoned freibergite.

The LA-ICP-MS data reveal that the pyrite from the three porphyry copper deposits/prospects have similar trace element compositions, as well as pyrite from the base metal veins. Analyzed pyrite crystals from the porphyry Cu deposits/prospects have

low As and Au contents and relatively high Se content. Measured chalcopyrite grains from these deposits also have high Se content and are depleted in Au and Ag. These results are consistent with the previously reported data for chalcopyrite from Elatsite by George et al. [61] and Gonzalez-Gimenez et al. [55]. Typical characteristics of the pyrite from the porphyry deposits/prospects are the high Co and Ni contents and low Ag, Cu, Pb and Sb contents. It seems that the fluids responsible for the porphyry Cu mineralization formation in the area were enriched in Se, Co and Ni. This is also supported by the observations of Petrunov et al. [48], Auge et al. [54] and Gonzalez-Gimenez et al. [55], who described selenides and Co-, Ni-thiospinels at Elatsite.

The pyrite samples from the base metal veins show higher As content and elevated Au content than those from the porphyry copper deposit/prospects. Comparable elevated As content in pyrite from the Elatsite deposit is reported by Krumov and Bogdanov [62] and Gonzalez-Gemenez et al. [55] from epithermal pyrite–galena–sphalerite association. The Au content in the pyrite from the base metal veins is highly variable and shows a positive correlation with As content. A similar positive Au/As correlation in pyrite has already been reported for Au-bearing arsenian pyrite from other hydrothermal deposits worldwide [6,14,15,63,64]. This correlation reflects the impact of arsenic in the speciation of Au in pyrite, i.e., incorporation either into the lattice as a solid solution or as micro- to nano-sized inclusions of Au-bearing minerals (Figure 10 after Reich et al. [64]; Keith et al. [14] and reference therein). According to Reich et al. [64], results plotting below the solubility curve should contain gold in solid solution, whereas those plotting above the solubility line should have Au as solid inclusions. All our data points from the three types of mineralization plots are below the solubility curve on the diagram, inferring that gold is present within the crystal lattice of the studied pyrite samples. Our results are concordant with the previously published data from porphyry Cu and epithermal Au deposits (Figure 10).

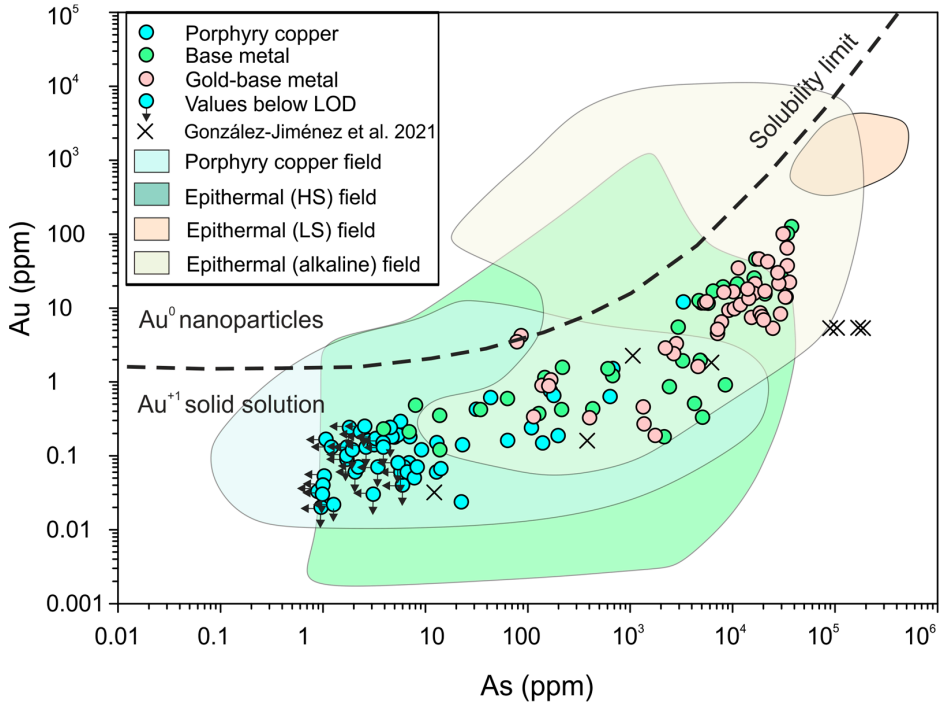

Figure 10. Content of Au vs. As in pyrite from the studied porphyry Cu deposit/prospects, base metal and gold-base metal veins from the Elatsite–Chelopech ore field based on LA-ICP-MS data. Published results from the Elatsite deposit by Gonzalez-Gimenez et al. [55]. Fields for porphyry Cu, high-sulfidation (HS) epithermal, low-sulfidation (LS) epithermal, alkaline rock-hosted epithermal deposits after Keith et al. [14] and references therein. The black dashed line defines the solubility limit for Au solid solution in pyrite as a function of As after Reich et al. [64].

Pyrite from the base metal veins also has higher Cu, Pb and Sb and lower Se contents compared to pyrtite from the porphyry Cu deposit/prospects, in agreement with the published dataset for the Ladolam Au deposit, where epithermal mineralization overprints porphyry style mineralization [6]. In pyrite from the base metal deposits, Co and Ni contents are comparable to those in pyrite from the porphyry copper deposits. Pyrite from the base metal veins is often formed together with arsenopyrite, which also has elevated Au, Co and Ni contents.

Cobalt is also detected in shalerite from the base metal veins with values up to 35 ppm. The time-resolved depth profiles for Co are always flat, suggesting homogeneous distribution in the sphalerite lattice without any evidence for sub-microscopic Co-bearing inclusions.

Lead isotopic compositions of sulfides from the three studied porphyry deposit/prospects and the spatially associated base metal veins of Negarshtitsa-West and Dolna Kamenitsa have very similar values. This reveals that both mineralization types belong temporally and genetically to the same metallogenic event and have a similar source of Pb and most probably of the other metals. As the lead isotopic characteristics of the porphyry copper and the base metal deposits are similar to that of the Late Cretaceous magmatic rocks, the most plausible interpretation is that Pb is of magmatic origin and that it was directly released by the Late Cretaceous magmas. The magmatic source of fluids, responsible for the formation of sulfides from these deposits, is also suggested by the sulfur isotopes of sulfide minerals. Our sulfur isotope results are compared with published sulfur isotope variation for the Svishti Plaz [59] and Chelopech deposits [60], as well as with the most typical values of $\delta^{34}S$ in sulfides from porphyry–copper deposits (Figure 9). There is good agreement in the variations of the sulfur isotopic data of the sulfide minerals from porphyry and base metal deposit/prospects of the Elatsite–Chelopech ore field with the most typical values of $\delta^{34}S$ in sulfides from porphyry–copper deposits (PCD field in Figure 9 after Hofstra and Cline [17]) that are genetically linked to magmatic fluids derived from calk–alkaline magmas (e.g., [1,65]).

5.2. Distal Gold-Base Metal Prospects

In all studied gold-base metal prospects, pyrite is As-bearing and contains Au as well. It is formed together with arsenopyrite, which is also Au-rich. Additionally, native gold is formed as part of the later base metal stage and precipitates in fractured pyrite and arsenopyrite or in quartz associated with the pyrite and arsenopyrite grains. Measured Au content in arsenopyrite from Svishti Plaz is comparable to the reported values by Dimitova et al. [66]. SEM analyses of arsenopyrite from the Svishti Plaz-Central part show that it is enriched in S (1.07–1.17 apfu) and depleted in As (0.87–0.92 apfu) in comparison to the stoichiometric composition. This is in agreement with the arsenopyrite compositions from Svishti Plaz previously published by Mladenova and Kerestedjian [67]. An arsenopyrite geothermometer [68,69] was applied with the objective to determine the formation temperature. Arsenopyrite is formed together with pyrite. Hence, the arsenic values ranging from 28.8 and 30.7 at. % fall in the "pyrite + arsenopyrite" zone of the buffered assemblages involving arsenopyrite in the Fe-As-S system (Figure 11). The calculated temperatures range from 285 °C to 358 °C. Bogdanov and Zairi [59] have determined temperatures between 230 °C and 320 °C for the pyrite–arsenopyrite and gold-base metal stages at Svishti Plaz, based on fluid inclusion study and sulfur isotope thermometry. We applied a galena–sphalerite thermometer in Kordunsko Dere based on S isotopes to determine the formation temperature of the later gold-base metal stage, according to Kajiwra and Krouse [70] and Liu et al. [71]. The calculated T values are 271 °C and 277 °C, respectively. The temperature of formation for the quartz–pyrite–galena–sphalerite assemblage at Elatsite is 230–240 °C, based on fluid inclusions study [51], which is lower than the calculated temperature interval for Kordunsko Dere.

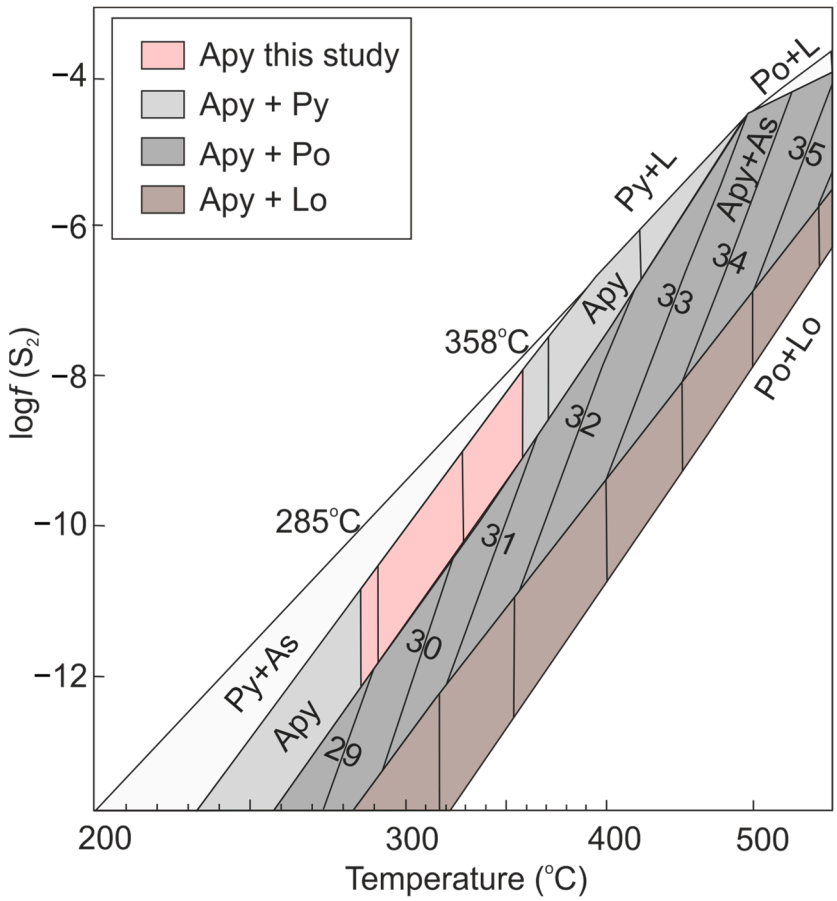

Figure 11. Activity of log $f(S_2)$ and temperature projection of the stability field of arsenopyrite from the Svishti Plaz gold-base metal veins after Kretschmar and Scott [68] and Sharp et al. [69].

Two elements that behave differently in pyrite from base metal and gold-base metal veins and that help to distinguish among them are Co and Ni. In pyrite from the base metal deposits, these elements have contents comparable to the pyrite from the porphyry copper deposits. On the other hand, the pyrite from the gold-base metal veins shows lower Co and Ni contents. Arsenopyrite from these deposits shows similar features.

Similarly, sphalerite from the gold-base metal veins also has lower Co content compared to sphalerite from the base metal veins but higher In and Cu contents. All LA-ICP-MS profiles for In are smooth, indicating homogeneous distribution and occurrence of the element in solid solutions. In some analyses, the spectra for Cu are ragged, showing clear evidence for Cu-bearing inclusions. Other profiles are flat, inferring solid solution copper. According to Cook et al. [72], some epithermal deposits appear to have higher contents of In in solid solutions where the ore is proximally positioned relative to the causative intrusive body. If we accept that the studied porphyry Cu, proximal base-metal and distal Au-base metal mineralization could be part of a single zonal porphyry system of the Late Cretaceous age, the In content in sphalerite from the distal gold-base metal deposits should be lower compared to those from the proximal base metal veins. However, our results show increased In content of sphalerite from the distal Au-base metal veins, compared to the proximal ones. This may be a sign that the former veins do not have the same origin in their magmatic–hydrothermal system.

Lead isotopic compositions of sulfides from gold-base metal veins differ significantly from those of sulfides from porphyry deposits and base metal veins. Based on model lead isotope ages, Amov et al. [19] and Amov [55] interpret these differences as evidence for different ages of the deposits: carboniferous for the gold-base metal prospects. Alternatively, the less evolved $^{206}Pb/^{204}Pb$ but higher $^{207}Pb/^{204}Pb$ isotope ratios in sulfides from gold-

base metal veins may reflect higher contamination with older continental crust. They may refer to longer circulation of fluids in the distal Au-base metal veins possibly resulting in greater contamination of the fluids during their longer passage through the basement rocks.

The sulfides of the gold-base metal veins show higher $\delta^{34}S$, compared to the sulfides from the porphyry copper and base metal deposits/prospects, although still falling in the typical magmatic range [73]. Our Pb and S isotope data for sulfides from Svishti Plaz are consistent with the previously published results by Amov et al. [19] and Bogdanov and Zairi [59]. Additionally, we analyzed Pb isotopes in sulfides from the adjacent Kordunsko Dere gold-base metal prospect, which show similar values to those of Svishti Plaz. The different Pb and S isotopic signature of sulfides from the Kordunsko Dere and Svishti Plaz-Central parts may suggest different mineralizing fluid source(s) in these veins.

6. Conclusions

In conclusion, we can summarize that pyrite, arsenopyrite and sulfosalt minerals from porphyry copper deposits, base-metal and gold-base metal veins are major carriers not only for Au but also for Ag, Sb, Se, and Co. Pyrite from the different types of mineralization in the northern part of the Panaguirishte district has specific geochemical characteristics. In the Elatsite–Chelopech ore field where dozens of porphyry copper and epithermal gold deposits, prospects and occurrences are known, and the geochemistry of pyrite could be used to discriminate among different mineralization types, especially in the areas without clear connections to any of the known deposits/prospects, when pyrite is part of a hydrothermal alteration formed at a distance from the main ore mineralization.

In addition to the close spatial relationships between the Elatsite and Gorna Kamenitsa porphyry Cu deposits and the Negarstitsa-West and Dolna Kamenitsa base metal prospects, as well as similarities in the mineralization and alteration styles (the upper marginal veins from the Elatsite deposit), the lead and sulfur isotopic signatures of sulfides support the idea of a genetic link between these two types of deposits. The porphyry and base-metal mineralization could be a result of a common ore-forming event during the Late Cretaceous.

Differing radiogenic lead and sulfur isotopic compositions of sulfides from distal gold-base metal veins of Kordunsko Dere, Svishti Plaz and Shipkite might be a consequence of the ore fluid interacting with an external older crustal and isotopically positive $\delta^{34}S$ source. Alternatively, a different fluid source for the formation of these gold-base metal veins could be suggested. A genetic relation to the Carboniferous granitoid magmatism might be considered, but this needs to be proved by reliable isotope dating techniques (e.g., Re-Os dating of arsenopyrite and pyrite).

Supplementary Materials: The following supporting information can be downloaded at: https://www.mdpi.com/article/10.3390/min13050630/s1, Table S1: Sample list and description; Table S2: AAA analyses of mineralized and altered samples; Table S3: ICP-AES and LA-ICP-MS whole-rock analyses; Table S4: SEM-EDS analyses of ore minerals; Table S5: LA-ICP-MS analyses of ore minerals.

Author Contributions: Conceptualization, E.S., I.P. and A.v.Q.; methodology, E.S., I.P., S.G., A.v.Q., A.B. and T.V.; formal analysis, E.S., I.P., S.G., A.v.Q., A.B. and T.V.; investigation, I.G., S.G., R.R. and P.M.; data curation, E.S., I.P., S.G., A.v.Q., A.B., T.V. and K.K.; writing—original draft preparation, E.S., I.P. and A.v.Q.; writing—review and editing, E.S., I.P., K.K. and P.M.; visualization, I.G., E.S., I.P. and A.v.Q. All authors have read and agreed to the published version of the manuscript.

Funding: This research was partly supported by the KP-06-N44/4 Project, financed by the Bulgarian National Science Fund.

Data Availability Statement: All data are contained within the article and supplementary materials.

Acknowledgments: We would like to thank the management of the Elatsite mine for providing access to the mine. We are also grateful to geologists from the mine for assistance in the field. We thank Tim Ireland and Clive Bonsall for correcting the manuscript for grammar and style. This work was supported by the KP-06-N44/4 Project, funded by the Bulgarian National Science Fund.

Conflicts of Interest: The authors declare no conflict of interest. The funders had no role in the design of the study; in the collection, analyses, or interpretation of data; in the writing of the manuscript, or in the decision to publish the results.

References

1. Sillitoe, R.H. Porphyry Copper Systems. *Econ. Geol.* **2010**, *105*, 3–41. [CrossRef]
2. Kouzmanov, K.; Moritz, R.; von Quadt, A.V.; Chiaradia, M.; Peytcheva, I.; Fontignie, D.; Ramboz, C.; Bogdanov, K. Late Cretaceous porphyry Cu and epithermal Cu–Au association in the Southern Panagyurishte District, Bulgaria: The paired Vlaykov Vruh and Elshitsa deposits. *Miner. Deposita* **2009**, *44*, 611–646. [CrossRef]
3. Pudack, C.; Halter, W.E.; Heinrich, C.A.; Pettke, T. Evolution of Magmatic Vapor to Gold-Rich Epithermal Liquid: The Porphyry to Epithermal Transition at Nevados de Famatina, Northwest Argentina. *Econ. Geol.* **2009**, *104*, 449–477. [CrossRef]
4. Chang, Z.S.; Hedenquist, J.W.; White, N.C.; Cooke, D.R.; Roach, M.; Deyell, C.L.; Garcia, J., Jr.; Gemmell, J.B.; Mcknight, S.; Cuison, A.L. Exploration tools for linked porphyry and epithermal deposits: Example from the Mankayan intrusion-centered Cu-Au District, Luzon, Philippines. *Econ. Geol.* **2011**, *106*, 1365–1398. [CrossRef]
5. Rinne, M.L.; Cooke, D.R.; Harris, A.C.; Finn, D.J.; Allen, C.M.; Heizler, M.T.; Creaser, R.A. Geology and geochronology of the Golpu porphyry and Wafi epithermal deposit, Morobe Province, Papua New Guinea. *Econ. Geol.* **2018**, *113*, 271–294. [CrossRef]
6. Sykora, S.; Cooke, D.R.; Meffre, S.; Stephanov, A.S.; Gardner, K.; Scott, R.; Selley, D.; Harris, A.C. Evolution of pyrite trace element com- positions from porphyrystyle and epithermal conditions at the Lihir gold deposit: Implications for ore genesis and mineral processing. *Econ. Geol.* **2018**, *113*, 193–208. [CrossRef]
7. Cooke, D.R.; Baker, M.; Hollings, P.; Sweet, G.; Chang, Z.; Danyushevsky, L.; Gilbert, S.; Zhou, T.; White, N.; Gemmell, J.B.; et al. New Advances in Detecting the Distal Geochemical Footprints of Porphyry Systems Epidote Mineral Chemistry as a Tool for Vectoring and Fertility Assessments. In *Building Exploration Capability for the 21st Century*; Kelley, K.D., Golden, H.C., Eds.; Colt Print Services: Boulder, CO, USA, 2014; pp. 127–152; ISBN 978-1-629491-424.
8. Mao, M.; Rukhlov, A.S.; Rowins, S.M.; Spence, J.; Coogan, L.A. Apatite trace element compositions: A robust new tool for mineral exploration. *Econ. Geol.* **2016**, *111*, 1187–1222. [CrossRef]
9. Cooke, D.R.; Agnew, P.; Hollings, P.; Baker, M.; Chang, Z.; Wilkinson, J.J.; White, N.C.; Zhang, L.; Thompson, J.; Gemmell, J.B.; et al. Porphyry indicator minerals (PIMS) and porphyry vectoring and fertility tools (PVFTS)–indicators of mineralization styles and recorders of hypogene geochemical dispersion halos. In Proceedings of the Exploration 17: Sixth Decennial International Conference on Mineral Exploration, Toronto, ON, Canada, 22–25 October 2017.
10. Sievwright, R. Developing Magnetite Chemistry as an Exploration Tool for Porphyry Copper Deposits. Ph.D. Thesis, Imperial College London, London, UK, 2017; 340p.
11. Wilkinson, J.J.; Baker, M.J.; Cooke, D.R.; Wilkinson, C.C.; Inglis, S. Exploration Targeting in Porphyry Cu Systems Using Propylitic Mineral Chemistry A Case Study of the El Teniente Deposit, Chile. *Econ. Geol.* **2020**, *115*, 771–791. [CrossRef]
12. Cook, N.J.; Ciobanu, C.L.; Mao, J. Textural control on gold distribution in As-free pyrite from the Dongping, Huangtuliang and Hougou gold deposits, North China Craton (Hebei Province, China). *Chem. Geol.* **2009**, *264*, 101–121. [CrossRef]
13. Deditius, A.P.; Reich, M.; Kesler, S.E.; Utsunomiya, S.; Chryssoulis, S.L.; Walshe, J.; Ewing, R.C. The coupled geochemistry of Au and As in pyrite from hydrothermal ore deposits. *Geochim. Cosmochim. Acta* **2014**, *140*, 644–670. [CrossRef]
14. Keith, M.; Smith, D.J.; Jenkin, G.R.T.; Holwell, D.A.; Dye, M.D. A review of Te and Se systematics in hydrothermal pyrite from precious metal deposits: Insights into ore-forming processes. *Ore Geol. Rev.* **2018**, *96*, 269–282. [CrossRef]
15. Large, R.R.; Danyushevsky, L.V.; Hollit, C.; Maslennikov, V.; Meffre, S.; Gilbert, S.E.; Bull, S.; Scott, R.J.; Emsbo, P.; Thomas, H.; et al. Gold and trace element zonation in pyrite using a laser imaging technique: Implications of the timing of gold in orogenic and Carlin-style sediment-hosted deposits. *Econ. Geol.* **2009**, *104*, 635–668. [CrossRef]
16. Gregory, M.J.; Lang, J.R.; Gilbert, S.; Hoal, K.O. Geometallurgy of the Pebble porphyry Cu-Au-Mo deposit, Alaska: Implications for gold distribution and paragenesis. *Econ. Geol.* **2013**, *108*, 463–482. [CrossRef]
17. Hofstra, A.H.; Cline, J.S. Characteristics and Models for Carlin-Type Gold deposits. In *Gold in 2000*; Hagemann, S.G., Brown, P.E., Eds.; Society of Economic Geologists: Littleton, CO, USA, 2000; pp. 163–220.
18. Reich, M.; Deditius, A.; Chryssoulis, S.; Li, J.-W.; Ma, C.-Q.; Parada, M.A.; Barra, F.; Mittermayr, F. Pyrite as a record of hydrothermal fluid evolution in porphyry copper system: A SIMS/EMPA trace element study. *Geochim. Cosmochim. Acta* **2013**, *104*, 42–62. [CrossRef]
19. Amov, B.; Arnaudov, V.; Pavlova, M.; Dragov, P.; Baldjieva, T.; Evstatieva, S. Lead isotope data on the Paleozoic granitoids and ore mineralizations from the Western Balkan Mountains and the Tran District (West Bulgaria). I. Isotopic ratios and geochronology. *Geol. Balc.* **1981**, *11*, 3–26.
20. Ciobanu, C.L.; Cook, N.G.; Stain, H. Regional setting and geochronology of the Late Cretaceous Banatitic Magmatic and Metallogenic Belt. *Miner. Depos.* **2002**, *37*, 541–567. [CrossRef]
21. Heinrich, C.A.; Neubauer, F. Cu-Au-Pb-Zn-Ag metallogeny of the Alpine-Balkan-Carpathian-Dinaride geodynamic province. *Miner. Depos.* **2002**, *37*, 533–540. [CrossRef]
22. Gallhofer, D.; Quadt, A.V.; Peytcheva, I.; Schmid, S.M.; Heinrich, C.A. Tectonic, magmatic, and metallogenic evolution of the Late Cretaceous arc in the Carpathian-Balkan orogen. *Tectonics* **2015**, *34*, 1813–1836. [CrossRef]

23. Peycheva, I.; von Quadt, A. The Palaeozoic protoliths of Central Srednogorie, Bulgaria: Records in zircons from basement rocks and Cretaceous migmatites. In Proceedings of the 5th International Symposium on Eastern Mediterranean Geology, Thessaloniki, Greece, 14–20 April 2004; p. T11-9.
24. Georgiev, S.; Gerdjikov, I.; Peytcheva, I.; Makaveev, P. Time frame of the Carboniferous tectonic and magmatic activity in the area of Vezhen pluton, Bulgaria. In Proceedings of the National Conference with International Participation "GEOSCIENCES 2020", Sofia, Bulgaria, 3–4 December 2020; Bulgarian Geological Society: Sofia, Bulgaria, 2020; Volume 81, pp. 72–74.
25. Dabovski, C.; Zagorchev, I.; Rouseva, M.; Chounev, D. Paleozoic granitoides in the Sushtinska Sredna Gora. *Ann UGP* **1972**, *16*, 57–92. (In Bulgarian)
26. Kamenov, B.; von Quadt, A.; Peytcheva, I. New insight into petrology, geochemistry and dating of the Vejen pluton, Bulgaria. *Geochem. Miner. Petrol.* **2002**, *39*, 3–25.
27. Carrigan, C.W.; Mukasa, S.B.; Haydoutov, I.; Kolcheva, K. Age of Variscan magmatism from the Balkan sector of the Orogen, central Bulgaria. *Lithos* **2005**, *82*, 125–147. [CrossRef]
28. Audetat, A.; Simon, A. Magmatic Controls on Porphyry Copper Genesis. *Econ. Geol.* **2012**, *16*, 553–572.
29. Antonov, M.; Gerdjikov, S.; Metodiev, L.; Kiselinov, C.; Sirakov, V.; Valev, V. *Explanatory Note to the Geological Map of the Republic of Bulgaria Scale 1:50,000*; Map Sheet K-35-37-B Pirdop, 2010, Geocomplex, Sofia; Ministry of Environment and Water, Bulgarian Geological Survey: Sofia, Bulgarian, 2008; pp. 1–99.
30. Kounov, A.; Gerdjikov, I.; Vangelov, D.; Balkanska, E.; Lazarova, A.; Georgiev, S.; Blunt, E.; Stockli, D. First thermochronological constraints on the Cenozoic extension along the Balkan fold-thrust belt (Central Stara Planina Mountains, Bulgaria). *Int. J. Earth Sci.* **2018**, *107*, 1515–1538. [CrossRef]
31. Gerdjikov, I.; Georgiev, N. *Spectacular Fabric but Little Displacement: Early Alpine Shear Zones from Zlatishka Stara Planina, Central Balkanides*; Bulgarian Geological Society: Sofia, Bulgaria, 2005; pp. 35–38.
32. Gerdjikov, I.; Georgiev, N. The Svishti plaz allochthone (Central Balkanides): Position and associated fabric. *Comptes Rendus-Acad. Bulg. Sci.* **2006**, *59*, 631–638.
33. Lazarova, A.; Gerdjikov, I.; Georgiev, N.; Dimov, D. The Anton shear zone (Central Stara planina Mountains). Temporal relations, extent and significance. *Comptes Rendus-Acad. Bulg. Sci.* **2006**, *59*, 639–644.
34. Vangelov, D.; Gerdjikov, Y.; Kounov, A.; Lazarova, A. The Balkan Fold-Thrust Belt: An overview of the main features. *Geol. Balc.* **2013**, *42*, 29–47. [CrossRef]
35. Stoykov, S.; Pavlishina, P. New data for Turonian age of the sedimentary and volcanic succession in the southeastern part of Etropole Stara Planina Mountain, Bulgaria. *Comptes Rendus-Acad. Bulg. Sci.* **2003**, *56*, 55–60.
36. Chambefort, I.; Moritz, R. Subaqueous environment and volcanic evolution of the Late Cretaceous Chelopech Au–Cu epithermal deposit, Bulgaria. *J. Volcanol. Geotherm. Res.* **2014**, *289*, 1–13. [CrossRef]
37. von Quadt, A.; Peytcheva, I.; Kamenov, B.; Fanger, L.; Heinrich, C.; Frank, M. The Elatsite porphyry copper deposit in the Panagyurishte ore district, Srednogorie zone, Bulgaria: U-Pb zircon geochronology and isotope-geochemical investigations of magmatism and ore genesis. In *The Timing and Location of Major Ore Deposits in an Evolving Orogen*; Blundell, D.J., Neubauer, F., von Quadt, A., Eds.; Geological Society Special Publication: London, UK, 2002; pp. 119–135.
38. von Quadt, A.; Moritz, R.; Peytcheva, I.; Heinrich, C.A. Geochronology and geodynamics of Late Cretaceous magmatism and Cu-Au mineralization in the Panagyurishte region of the Apuseni-Banat-Timok-Srednogorie belt, Bulgaria. *Ore Geol. Rev.* **2005**, *27*, 95–126. [CrossRef]
39. Stoykov, S.; Peytcheva, I.; von Quadt, A.; Moritz, R.; Frank, M.; Fontignie, D. Timing and magma evolution of the Chelopech volcanic complex (Bulgaria). *Schweiz. Mineral. Petrogr. Mitt.* **2004**, *84*, 101–117.
40. Popov, K. Lithostratigraphy of the Late Cretaceous rocks in the Panagyurishte ore region. *Ann. Univ. Min. Geol.* **2005**, *48*, 101–114.
41. Kamenov, B.K.; Yanev, Y.; Nedialkov, R.; Moritz, R.; Peytcheva, I.; von Quadt, A.; Stoykov, S.; Zartova, A. Petrology of Upper Cretaceous island-arc ore-magmatic centers from the Central Srednogorie, Bulgaria: Magma evolution and paths. *Geochem. Miner. Petrol.* **2007**, *45*, 39–77.
42. Karagjuleva, J.; Kostadinov, V.; Tzankov, T.; Gočev, P. Structure of the Panagjurište strip east of the Topolnica River. *Bull. Geol. Inst. Bulg. Acad. Sci. Ser. Geotecton.* **1974**, *23*, 231–301. (In Bulgarian)
43. Gerdjikov, I.; Dinev, Y.; Vangelov, D. Structural geology of the central part of Kamenitsa-Rakovishka fault zone. *J. Min. Geol. Sci.* **2020**, *63*, 214–219.
44. Kounov, A.; Gerdjikov, I. The problems of the post-Cenomanian tectonic evolution of the central parts of the Sredna Gora Zone. The wrench tectonics—How real is real. *Geol. Balc.* **2020**, *49*, 39–58. [CrossRef]
45. Chambefort, I.; Moritz, R.; von Quadt, A. Petrology, geochemistry and U–Pb geochronology of magmatic rocks from the high-sulfidation epithermal Au–Cu Chelopech deposit, Srednogorie zone, Bulgaria. *Miner. Depos.* **2007**, *42*, 665–690. [CrossRef]
46. Guillong, M.; Meier, D.L.; Allan, M.M.; Heinrich, C.A.; Yardley, B.W.D. SILLS: A MATLAB-based program for the reduction of laser ablation ICP-MS data of homogeneous materials and inclusions. *Mineral. Assoc. Can. Short Course* **2008**, *40*, 328–333.
47. Fallick, A.E.; McConville, P.; Boyce, A.J.; Burgess, R.; Kelley, S.P. Laser microprobe stable isotope measurements on geological materials: Some experimental considerations (with special reference to δ34S in sulphides). *Chem. Geol.* **1992**, *101*, 53–61. [CrossRef]
48. Petrunov, R.; Dragov, P.; Ignatov, G.; Neikov, H.; Iliev, T.; Vasileva, N.; Tsatsov, V.; Djnakov, S.; Doncheva, K. Hydrotermal PGE-mineralisation in the Elatsite porphyry-copper deposit (Sredna Gora metallogenic zone, Bulgaria). *Comptes Rendus-Acad. Bulg. Sci.* **1992**, *45*, 37–40.

49. Dragov, P.; Petrunov, R. Elatzite porphyry copper-precious metals (Au and PGE) deposit. In *Plate Tectonic Aspects of the Alpine Metallogeny in the Carpatho–Balkan Region, Proceedings, Annual Meeting UNESCO-IGCP Project*; Popov, P., Ed.; USGS: Reston, VA, USA, 1996; pp. 171–175.
50. Fanger, L. Geology of a Porphyry Copper (-Au-PGE) Ore Deposit: Elatsite, Bulgaria. Master's Thesis, ETH Zürich, Zurich, Switzerland, 2001; 167p.
51. Strashimiriov, S.; Ptrunov, R.; Kanazirski, M. Porphyry-copper mineralization in the central Sred- nogorie zone. *Miner. Depos.* **2002**, *37*, 587–598. [CrossRef]
52. Georgiev, G. A genetic model of the Elatsite porphyry copper deposit, Bulgaria. *Geochem. Miner.Petrol.* **2008**, *48*, 143–160.
53. Tarkian, M.; Hünken, U.; Tokmakchieva, M.; Bogdanov, K. Precious-metal distribution and fluid-inclusion petrography of the Elatsite porphyry copper deposit, Bulgaria. *Miner. Depos.* **2003**, *38*, 261–281. [CrossRef]
54. Auge, T.; Petrunov, R.; Bailly, L. On the origin of the PGE mineralization in the Elatsite porphyry Cu-Au deposit, Bulgaria: Comparison with the Baula-Nuasahi Complex, India, and other alkaline PGE-rich porphyries. *Can. Miner.* **2005**, *43*, 1344–1372. [CrossRef]
55. González-Jiméneza, J.M.; Piña, R.; Kerestedjian, T.N.; Gervilla, F.; Borrajoe, I.; Farré-de Pablo, J.; Proenza, J.A.; Tornos, F.; Roquéf, J.; Nieto, F. Mechanisms for Pd-Au enrichment in porphyry-epithermal ores of the Elatsite deposit, Bulgaria. *J. Geochem. Explor.* **2021**, *220*, 106664. [CrossRef]
56. Mladenova, V.; Apostolova, R.; Ivanov, Z. Epithermal intermediate-sulfidation veins in the low-grade metamorphic rocks in the upper levels of the Elatsite porphyry copper deposit, Bulgaria. *Rev. Bulg. Geol. Soc.* **2017**, *78*, 41–54.
57. Stacey, J.S.; Kramers, J.D. Approximationof terrestrial Lead isotope evolution by a two-stage model. *Earth Planet. Scince Lett.* **1975**, *26*, 207–221. [CrossRef]
58. Amov, B. Lead isotope data of ore deposits from Bulgaria and the possibility for their use in archaeometry. *Berl. Beiträge Zur Archäometrie* **1999**, *16*, 5–19.
59. Bogdanov, K.B.; Zairi, N.M. Mineralogical and sulphur isotope study of Svishti Plaz deposit, Balkan Mountains, Bulgaria. In Proceedings of the 14th Congress of CBGA, Sofia, Bulgaria, September 1989; Sofia University Press: Sofia, Bulgaria, 1989; Volume 1, pp. 55–58.
60. Moritz, R.; Chambefort, I.; Chiaradia, M.; Fontignie, D.; Petrunov, R.; Simova, S.; Arisanov, A.; Doychev, P. The Late Cretaceous high-sulfidation Au–Cu Chelopech deposit, Bulgaria: Geological setting, paragenesis, fluid inclusion microthermometry of enargite, and isotope study (Pb, Sr, S). In *Mineral Deposits at the Beginning of the 21st Century, Proceedings 6th Biennial SGA Meeting, Krakow, Poland, 26–29 August 2001*; Piestrynski, A., Ed.; A.A. Balkema Publishers: Rotterdam, The Netherlands, 2001; pp. 547–550.
61. George, L.; Cook, N.; Crowe, B.; Ciobanu, C. Trace elements in hydrothermal chalcopyrite. *Mineral. Mag.* **2018**, *82*, 59–88. [CrossRef]
62. Krumov, I.; Bogdanov, K. Trace elements vectors in minerals from Elatsite PCD, Bulgaria. In Proceedings of the Annual Science Conference "GEOSCIENCES 2017", Sofia, Bulgaria, 7–8 December 2017; Bulgarian Geological Society: Sofia, Bulgaria, 2017; pp. 25–26.
63. Cook, N.J.; Chryssoulis, S.L. Concentrations of invisible gold in the common sulfides. *Can. Miner.* **1990**, *28*, 1–16.
64. Reich, M.; Kesler, S.E.; Utsunomiya, S.; Palenik, C.S.; Chryssoulis, S.L.; Ewing, R.C. Solubility of gold in arsenian pyrite. *Geochim. Cosmochim. Acta* **2005**, *69*, 2781–2796. [CrossRef]
65. Rye, R.O. A review of the stable-isotope geochemistry of sulfate minerals in selected igneous environments and related hydrothermal systems. *Chem. Geol.* **2005**, *215*, 5–36. [CrossRef]
66. Dimitrova, D.; Mladenova, V.; Sabeva, R.; Mofessie, A. Gold concentrations in arsenopyrite from the Govezhda and Svishti Plaz deposits, Bulgaria: A LA-ICP-MS study. In Proceedings of the National Conference with international participation "GEOSCIENCES 2012", Sofia, Bulgaria, 13–14 December 2012; Bulgarian Geological Society: Sofia, Bulgaria, 2017; pp. 17–18.
67. Mladenova, V.; Kerestedjian, T. The Svishti Plaz gold deposit, Central Balkan Mountains, Bulgaria. *Geochem. Miner. Petrol.* **2002**, *39*, 53–66.
68. Kretschmar, U.; Scott, S.D. Phase relations involving arsenopyrite in the system Fe-As-S and their application. *Can. Miner.* **1976**, *14*, 364–386.
69. Sharp, Z.D.; Essene, E.J.; Kelly, W.C. A re-examination of the arsenopyrite geobarometry: Pressure considerations and applications to natural assemblages. *Can. Miner.* **1985**, *23*, 517–534.
70. Kajiwra, Y.; Krouse, H.R. Sulfur isotope partitioning in metallic sulfide systems. *Can. J. Earth Sci.* **1971**, *8*, 1397–1408. [CrossRef]
71. Liu, S.; Li, Y.; Liu, J.; Shi, Y. First-principles study of sulfur isotope fractionation in pyrite-type disulfides. *Am. Min.* **2015**, *100*, 203–208. [CrossRef]
72. Cook, N.J.; Ciobanu, C.L.; Pring, A.; Skinner, W.; Shimisu, M.; Danyushevsky, L.; Saini-Eidukat, B.; Melcher, F. Trace and minor elements in sphalerite: A LA-ICPMS study. *Geochim. Cosmochim. Act.* **2009**, *73*, 4761–4791. [CrossRef]
73. Seal, R. Sulfur Isotope Geochemistry of Sulfide Minerals. *Rev. Mineral. Geochem.* **2006**, *61*, 633–677. [CrossRef]